



Published in final edited form as:

Sci Transl Med. 2023 May 31; 15(698): eabo3189. doi:10.1126/scitranslmed.abo3189.

PSMC3 proteasome subunit variants are associated with neurodevelopmental delay and type I interferon production

A full list of authors and affiliations appears at the end of the article.

Abstract

A critical step in preserving protein homeostasis is the recognition, binding, unfolding, and translocation of protein substrates by six AAA-ATPase proteasome subunits (ATPase Associated with various cellular Activities) termed PSMC1–6, which are required for degradation of proteins by 26S proteasomes. Here, we identified fifteen *de novo* missense variants in the *PSMC3* gene encoding the AAA-ATPase proteasome subunit PSMC3/Rpt5 in twenty-three unrelated heterozygous patients with an autosomal dominant form of neurodevelopmental delay and intellectual disability. Expression of *PSMC3* variants in mouse neuronal cultures led to altered dendrite development and deletion of the *PSMC3* fly ortholog Rpt5 impaired reversal learning capabilities in fruit flies. Structural modeling as well as proteomic and transcriptomic analyses of T cells derived from patients with *PSMC3* variants implicated the *PSMC3* variants in proteasome dysfunction through disruption of substrate translocation, induction of proteotoxic stress and alterations in proteins controlling developmental and innate immune programs. The proteostatic perturbations in T cells from patients with *PSMC3* variants correlated with a dysregulation in type I interferon (IFN) signaling in these T cells, which could be blocked by inhibition of the intracellular stress sensor, protein kinase R (PKR). These results suggest that proteotoxic

*Corresponding authors: elke.krueger@uni-greifswald.de, stephane.bezieau@chu-nantes.fr.

†The authors equally contributed to this work.

‡The authors equally contributed to this work.

Author contributions:

Patient enrolment was supervised by SK. Acquisition of genomic and clinical data was supervised by SK, TW, EEE and SB. The behavioural studies were designed, conducted and analysed by CR and FB. The structural modelling studies were carried out by VM and PWH. Facial image analysis of patients was made by TCH and PK. The in-vivo neuronal morphology assays were designed, performed and analysed by GMvW, CdK, SMWT and YE. The functional in vitro experiments on SHSY5Y cells and T cells were performed by FE, JJP, RG, TB, VV and WD and analysed by FE and EK. Proteomic investigations were conducted by EH and UV and analysed by EH, UV, MPSB and AD. Gene expression analysis by NanoString® was made by MST, FE and EK.

List of Supplementary Materials

Materials and Methods

Fig. S1 to S14

Table S1

Data Files S1

Uncropped Western blots

References (107–120)

Reproducibility Checklist

Competing interests: Authors declare that they have no competing interests.

Data and materials availability: All data associated with this study are present in the paper or the Supplementary Materials.

Drosophila lines are available from the Bloomington *Drosophila* Stock Center. Research Resource Identifiers (RRID) are provided in the Supplementary Materials and Methods. The mass spectrometry proteomics data have been deposited to the ProteomeXchange Consortium via the PRIDE partner repository with the dataset identifier PXD041182. Data sets from transcriptomics analysis (NanoString) has been deposited to the GEO repository under accession number GSE228675. Plasmids generated in this study can be provided by E.K. under a Universitaetsmedizin Greifswald Material Transfer agreement. Human cells derived from Patients #13, #17, #18 and #21 are stored in the University Medicine Greifswald Biobank. Availability of patient's samples is restricted depending on patient's consents for follow-up analysis.

stress activated PKR in patient-derived T cells resulting in a type I IFN response. The potential relationship among proteasome dysfunction, type I IFN production and neurodevelopment suggest new directions in our understanding of pathogenesis in some neurodevelopmental disorders.

INTRODUCTION

Proteasomes are large multi-protein complexes whose structure is adapted to the function of regulated protein degradation, thereby controlling many cellular processes (1, 2). Together with the autophagosomal-lysosomal system, proteasomes maintain protein homeostasis by counterbalancing the synthesis of new proteins by the translational machinery (3–6). The proteasome is part of the ubiquitin-proteasome system (UPS) which counts numerous enzymes acting upstream of the proteasome (7, 8). Aged or unstructured proteins are preliminary ubiquitin-tagged by the ubiquitination machinery through a cascade of enzymatic reactions for degradation by the 26S proteasome (9, 10). The 26S proteasome consists of two parts, the 20S core proteolytic particle and the 19S regulatory particle which caps the 20S particle at one or both ends (11, 12). Polyubiquitinated proteins are recognized by the 19S regulatory particle which comprises two parts: a base and a lid. In the base, four regulatory particle non-ATPase (Rpn) subunits (Rpn1, Rpn2, Rpn10 and Rpn13; encoded by the proteasome genes *PSMD2*, *PSMD1*, *PSMD4* and *ADRM1*, respectively) ensure recognition and capture of ubiquitin-modified substrates (13, 14). The lid contains eight additional non-ATPase subunits Rpn3, Rpn5–9, Rpn12, and Rpn15 which serve as scaffolds for binding of other subunits (15, 16) and the deubiquitinating enzyme Rpn11 (encoded by *PSMD14*) (17). Six AAA-ATPase subunits (Rpt1–6), encoded by the genes *PSMC1–6* in the base use the energy provided by ATP hydrolysis to unfold and translocate the substrate into the barrel-shaped 20S proteolytic core particle by gate opening. The 20S complex comprises heptameric α - and β -rings with an $\alpha_{1-7}\beta_{1-7}\beta_{1-7}\alpha_{1-7}$ architecture encoded by proteasome alpha subunit *PSMA1-7* or beta subunit genes *PSMB1-7*. The β -ring may be subjected to variations, thereby giving rise to two major proteasome isoforms, namely standard- and immunoproteasomes. Standard proteasomes typically contain the catalytic $\beta 1$, $\beta 2$ and $\beta 5$ subunits with caspase-, trypsin- and chymotrypsin-like activities, respectively (18, 19). In immunoproteasomes, the $\beta 1$, $\beta 2$ and $\beta 5$ subunits are replaced by the inducible $\beta 1i$, $\beta 2i$ and $\beta 5i$ subunits, encoded by the *PSMB9*, *PSMB10* and *PSMB8* genes, respectively (20). Although standard proteasomes are expressed in virtually all types of tissues, the expression of the inducible β -subunits is restricted to immune cells and non-immune cells exposed to type I or II interferons (IFNs) (21, 22).

Pathogenic variants in proteasome subunit genes cause rare proteasomopathies with a broad spectrum of symptoms (23, 24). So far, with the exception of the *PSMB1* ($\beta 6$) subunit (25), all pathogenic variants related to the 20S core particle have been shown to provoke immune dysregulation. Indeed, several genes encoding β -subunits (*PSMB4*, *PSMB8*, *PSMB9*, *PSMB10*), α -subunits (*PSMA3*) or assembly chaperone genes (proteasome maturation protein *POMP*, proteasome assembly chaperone Pac2 gene *PSMG2*) of the 20S proteasome complex have been involved in autosomal recessive proteasome-associated autoinflammatory syndromes (PRAAS) typically characterized by persistent type I IFN signaling (26–33). By contrast, genetic disorders involving genes of the 19S

regulatory particle such as the Stankiewicz-Isidor syndrome (STISS, MIM: 617516) caused by truncating variants of *PSMD12* (also referred to as Rpn5) are neurodevelopmental polymalformative syndromes (34) with subclinical activation of type I IFN signaling (35, 36) These observations place both PRAAS and STISS in the category of type I interferonopathies, a recent family of genetically determined rare autoinflammatory syndromes with dysregulated type I IFN signaling that includes Aicardi-Goutières syndrome and familial chilblain lupus (37, 38). Clinically, these diseases are complex, demonstrating multiple organ involvement (often brain and skin), encompassing a broad range of phenotypes and being associated with high morbidity and mortality (39). In this work, we identified fifteen dominant *de novo* variants in the *PSMC3* gene coding for the AAA-ATPase PSMC3/Rpt5. These rare missense variants were detected in twenty-three individuals presenting with neurodevelopmental delay (NDD), intellectual disability (ID) or both, together with various congenital malformations. Together, our data highlight interferonopathy as a potential contributor to the pathogenesis of NDD/ID in patients carrying loss-of-function variants in subunits of the 19S proteasome regulatory particle and identify protein kinase R (PKR) as a major player in disease pathogenesis.

RESULTS

Identification of *PSMC3* variants

The first *PSMC3* variant was detected in Patient #2, a female newborn presenting with severe cardiac, gastrointestinal, inflammatory and immune issues. Whole-exome sequencing (WES) highlighted the *de novo* nonsynonymous c.523A>G p.(M175V) variant (GenBank ID: NM_002804.4) which was absent in any public variant databases (gnomAD, >246,000 chromosomes; NHLBI Exome Variant Server, >13,000 alleles; Bravo, 125,568 alleles) and predicted to be pathogenic by bioinformatics programs including SIFT, PolyPhen-2n CADD, REVEL, and Metadome as well as all programs compiled by MobiDetails (40). Our overall strategy described in the Materials and Methods allowed us to identify a total of 15 distinct rare *de novo* missense *PSMC3* variants in 23 unrelated children presenting with a syndrome characterized by neurodevelopmental delay (NDD) and various congenital anomalies (Table 1).

As shown in Fig. 1, most of the *PSMC3* substitutions were localized in the AAA domain that was predicted to be intolerant to variations (Fig. S1). Two distinct regions of the AAA domain were particularly prone to substitutions. The first hotspot was centered on the recurrent variant c.910C>T p.(R304W) detected in four unrelated children and encompassed variants c.910C>G p.(R304G), c.915G>T p.(E305D) and c.929T>C p.(M310T) (Fig. 1). The second region, enriched in rare variants [c.775A>G p.(M259V), c.776T>C p.(M259T), c.782T>C p.(I261T) -seen six times-, c.784G>A p.(G262R) and c.806G>C p.(R269P)], was more N-terminally located (Fig. 1). All thirteen affected residues were highly conserved across species from mammals down to fission yeast (Fig. 1). One major phenotypic hallmark of all individuals carrying *PSMC3* variants was the predominance of neurodevelopmental or neuropsychiatric symptoms (Table S1). In more detail, apart from Patient #2, all affected children exhibited developmental delay (22/22; 100%) characterized by speech delay (19/19; 100%) alone or with intellectual disability (16/18; 89%) as well

as motor delay (15/19; 79%). Brain magnetic resonance imaging highlighted frequent anomalies (11/15; 73%), whereas the occurrence of abnormal behavior (9/18; 50%) and seizures (5/21; 24%) varied. Nine of 19 (47%) individuals experienced growth failure, most with feeding difficulties (8/18; 44%). Malformations were frequently observed in the skeleton [11/15; 73%; scoliosis, acetabular dysplasia, brachymetatarsy), heart (10/18; 56%; ventricular or septal defects, patent ductus arteriosus, pulmonary hypertension and atresia), kidney (4/15; 27%; horseshoe shape, pelvicalyceal dilatation, nephrocalcinosis, and multi-cystic dysplastic kidney), and head (microcephaly in 6/17 (35%); relative to severe macrocephaly in 2/16 (13%)]. Tumors were noted in 2/19 (11%) individuals (craniopharyngioma and neuroblastoma). Hearing loss was detected in 9/19 individuals (47%) and labeled as sensorineural in two and conductive in one of them, respectively. Most of the children (18/20; 90%) displayed dysmorphic facial features (Fig. S2), including tall or broad forehead (7/19; 37%), thin upper lip with down-turned corners of mouth (6/19; 32%), abnormal palate (5/19; 265/19; 26%), epicanthal folds (5/19; 26%), and orofacial clefts (2/19; 10%). Computational analysis of facial morphology by GestaltMatcher (41) revealed that facial dysmorphism among the patients carrying *PSMC3* variants was rather heterogeneous with similarities only observed between patients carrying identical variants (Fig. S2).

Silencing of the *PSMC3 Drosophila* ortholog Rpt5 in adult flies fails to reverse stimulus contingencies

Given the neuronal nature of the phenotype of patients carrying *PSMC3* variants, we next sought to address the potential involvement of *PSMC3* in cognitive function by evaluating the learning performance of *Drosophila melanogaster* fruit flies with a RNAi knockdown of Rpt5 (*Drosophila* ortholog of human *PSMC3*) expression by two different siRNAs, namely Rpt5³²⁴²² and Rpt5⁵³⁸⁸⁶ targeting Rpt5 transcripts at two different sites. To this end, we used a standard conditioning of odor-avoidance paradigm, in which animals were exposed to two different odors (3-octanol, OCT or 4-methylcyclohexanol, MCH), only one of which resulted in the simultaneous application of a foot-shock (OCT⁺, MCH⁻), as previously described (42) (Fig. 2A and B). Silencing of Rpt5 using Rpt5 RNAi under control of the neuron specific embryonic lethal abnormal visual system (Elav) promoter resulted in no significant differences in learning performance for Rpt5³²⁴²² (WT vs. Elav:RPT5³²⁴²², P=0.6435, N=4) or Rpt5⁵³⁸⁸⁶ (WT vs. Elav:RPT5⁵³⁸⁸⁶, P=0.5282, N=6) siRNAs (Fig. 2C). We next determined the reversal learning performance of Rpt5-silenced flies by training with an initial odor shock pairing (OCT⁺, MCH⁻) immediately followed by training with a reversed odor shock pairing (OCT⁻, MCH⁺) (Fig. 2B, lower panel). Reversal learning performance was significantly poorer with pan-neuronal Rpt5 RNAi expression of Rpt5³²⁴²² (WT vs. Elav:RPT5³²⁴²², P<0.0001, N=4) or Rpt5⁵³⁸⁸⁶ (WT vs. Elav:RPT5⁵³⁸⁸⁶, P=0.0022, N=6) siRNAs. The three control groups once again did not significantly differ from each other (Fig. 2C). These data suggest that *PSMC3* ortholog Rpt5 appears as a prerequisite for the changes in learned associations in *Drosophila melanogaster*.

Ectopic expression of PSMC3/Rpt5 or its variants differentially impact neuronal development

In view of the negative impact of *PSMC3/Rpt5* gene silencing on reversal learning, we next asked whether *PSMC3* was involved in the regulation of hippocampal neuron dendritic development. We therefore ectopically expressed wild-type PSMC3/Rpt5 in murine primary hippocampal neurons prior to neurite length quantification, as previously described (43). As shown in Fig. S3, expression of wild-type PSMC3/Rpt5 at an early developmental time point *in vitro* [Day In Vitro (DIV) 3] resulted in significantly reduced neurite length of the neurons (empty vector vs PSMC3 WT, $p=0.0089$). These results suggested that ectopic expression of wild-type PSMC3/Rpt5 may be detrimental to neurite outgrowth. We next sought to determine whether the different PSMC3/Rpt5 variants identified in patients with NDD/ID behaved differently compared to wild-type PSMC3/Rpt5 in neurons when ectopically expressed. Expression of the R304W, E305D and E383L PSMC3/Rpt5 variants resulted in similar neuronal morphological changes as seen with wild-type PSMC3/Rpt5 (Fig. S3). By contrast, expression of the M175V variant did not affect neuronal morphology when compared to the empty vector control, and showed significant improvement when compared to wild-type PSMC3/Rpt5 (Fig. S3). The positive effects exerted by the M175V PSMC3/Rpt5 variant on neurite length and arborization are intriguing but do not reflect an increased ability of the mutant subunit to incorporate into 19S-capped proteasome complexes (Fig. S4). In addition, these observations do not preclude a milder pathogenicity of this variant, because the morphological changes seen are not necessarily beneficial for neurite outgrowth. Taken together these results suggest that PSMC3/Rpt5 participates in the regulation of neurite development and that any alteration of this gene might affect this process positively or negatively.

PSMC3 gene variants differentially affect PSMC3/Rpt5 steady-state protein expression

Because missense variants may cause haploinsufficiency by affecting mRNA and/or protein turnover, we next sought to determine the impact of the identified *PSMC3* variants on PSMC3/Rpt5 steady-state protein expression. To this end, thirteen of the *PSMC3* variants were expressed in the SHSY5Y neuroblastoma cell line with a fused N-terminal hemagglutinin (HA) tandem repeat prior to Western-blot analysis. As shown in Fig. 3A, the four PSMC3/Rpt5 variants carrying the R171W, A237V, M259V and I261T mutations exhibited lower PSMC3/Rpt5 protein expression than their wild-type counterpart. Densitometric analysis of the HA-PSMC3 bands (Fig. 3A, lower left panel) and of PSMC3 bands (Fig. 3A, lower right panel) emerging from these constructs revealed that PSMC3/Rpt5 protein expression was reduced by about 90% when compared to wild-type HA-PSMC3 (Fig. 3A). However, all *PSMC3* variants generated equivalent amounts of HA-*PSMC3* transcripts in SHSY5Y cells in a 24-h plasmid-driven expression, as determined by RT-PCR and densitometric quantification (Fig. 3B), thereby indicating that reduced protein expression was due to increased protein turnover, decreased translation efficiency, or both. To determine whether these effects could be caused by non-pathogenic *PSMC3* mutations as well, we next analyzed the steady-state expression of three HA-tagged single nucleotide polymorphisms (SNPs) PSMC3/Rpt5 variants (I77N, I291V and P355L) reported in the Genome Aggregation Database (gnomAD). As shown in Fig. S5, the three investigated

SNPs behaved similarly to their wild-type counterpart, suggesting that decreased *PSMC3*/*Rpt5* protein expression may be a specific feature of some pathogenic variants.

Ectopic expression of HA-*PSMC3*/*Rpt5* fusion proteins in SHSY5Y cells was accompanied by expression of untagged *PSMC3*/*Rpt5* (Figs. 3A and S5). One potential explanation for this observation implies a partial destruction of the HA epitope, as previously described (44). This assumption is, however, not supported by the fact that such phenomenon was not observed when other proteasomes AAA-ATPases such as *PSMC5*/*Rpt6* were N-terminally tagged with the same HA epitope (Fig. S6). Rather, it may be that the increased pools of untagged *PSMC3*/*Rpt5* detected in cells expressing HA-*PSMC3*/*Rpt5* might reflect a stabilization of endogenous *PSMC3*/*Rpt5*. Overexpressed and endogenous *PSMC3*/*Rpt5* proteins might undergo self-association resulting in the formation of homomers protecting them from degradation. To address this point, HA-*PSMC3*/*Rpt5* fusion proteins were pulled down from SHSY5Y cells using HA antibody followed by Western-blot analysis for *PSMC3*/*Rpt5*. As shown in Fig. S7, HA-*PSMC3* coprecipitated with untagged *PSMC3*/*Rpt5*, thereby confirming physical interaction between overexpressed and endogenous *PSMC3*/*Rpt5*. However, although the regulation of *PSMC3*/*Rpt5* subunit in response to concentration changes is potentially interesting, the observation that this feature does not vary between wild-type and stable *PSMC3* variants suggests that this is not relevant to disease pathogenesis. Altogether, these data showed that the *PSMC3* missense variants identified in patients with NDD/ID differentially impact protein expression and stability.

Structural modeling predicts that *PSMC3* substitutions affect inter and intra-molecular interactions between proteasome subunits

We next attempted to predict the structural consequences of each of the fourteen *PSMC3* substitutions by assessing the localization of the mutated residues in the human 26S proteasome structure generated by Dong et al. (Protein Data Bank, PDB-entry code: 6MSK) (45). Most of the affected amino acids emerged within the N-terminal α/β domain of *PSMC3*/*Rpt5* with five residues (G262, I261, M259, R304 and E305) residing in two loops adjacent to the substrate tunnel pointing towards the center of the AAA-ATPase ring (Figs. 3C and D). Specifically, on one loop, G262 was fixed by a main chain hydrogen bond to E305, thereby promoting flexibility of the preceding loop containing M259. Besides, E305 itself was held through a salt bridge by R308 with its preceding residue R304 involved in a polar network stabilizing the neighbouring loop (Fig. S8). Because these six residues stabilized or were part of the tertiary structure of the loops, any alteration of these amino acids is predicted to affect substrate trafficking, as well as interactions with other AAA-ATPase subunits. As shown in Fig. S8, the A237V variant was more difficult to classify and did not reveal itself structurally at first sight. However, one cannot exclude that the slight increase in residue size at position 237 might lead to structural changes. The overexpression assays in SHSY5Y cells suggest that such substitution does affect sidechain packing and protein stability (Fig. 3A). The E383L missense variant was the only substitution lying within the C-terminal α -helical domain of *PSMC3*/*Rpt5* adjacent to the 19S-20S interface. E383 held Q166 from the PSMA1/ α 6 subunit for polar interactions with both of the R169 and R386 residues (Fig. 3E). Changing the negatively charged E383 to a positively charged K383 is therefore predicted to disrupt such hydrogen bond network

and affect the association of the 19S complex with the 20S core particle. E287 was also located in close proximity to the ATP binding site (Fig. S8) and its substitution with Q287 presumably generated additional polar bonds with N333 likely to affect ATP binding, hydrolysis, or both. R171 was positioned at the PSMC3/Rpt5-PSMC2/Rpt1 interface and was part of a polar network involving the neighboring D169 and Q258 residues (Fig. S9). As such, the substitution of positively charged arginine to hydrophobic tryptophan at this position is predicted to disrupt these interactions, and a fortiori to affect the contact between the two subunits (Fig. S9). The change of M175 to V175 resulted in the loss of a polarized thiol group and hydrophilic environment which was likely to destabilize the tertiary structure of this protein region (Fig. S9). Taken together, these data suggest that the complex 26S proteasome structure may be strongly affected by the identified *PSMC3* missense variants, even though an incorporation of dysfunctional PSMC3/Rpt5 subunit with no detrimental effects of proteasome structure cannot be fully excluded.

***PSMC3* variants differentially impact proteasome assembly**

To further address the pathogenicity of the *PSMC3* variants, T cells from Patients #13, #18 and #21 were analyzed for their proteasome contents. The intracellular expression of the $\alpha 7$ proteasome subunits and PA28- α did not vary between relative controls (father, mother or both) and index cases (Fig. 4A). Likewise, the abundance of the 19S subunit PSMD12/Rpn5 in mutant T cells was comparable to that detected in their control counterparts. T cells expanded from controls and patients exhibited two prominent PSMC3/Rpt5 immunoreactive bands migrating at about 50 and 40 kDa (Fig. 4A). Although the upper band running at ~50 kDa corresponded to PSMC3/Rpt5 expected size, the nature of the lower band running at ~40 kDa was unclear. It is, however, unlikely that this band may be non-specific, because it was detectable in T cells using another anti-PSMC3/Rpt5 antibody or in other cell types (Fig. S10). This additional species might reflect a shorter, as yet undescribed PSMC3/Rpt5 isoform or a processed form arising from the PSMC3/Rpt5 full-length protein. Nevertheless, the unchanged protein expression profile of PSMC3/Rpt5 between controls and patients indicates that none of these phenomena is affected by any of the *PSMC3* variants. Likewise, none of *PSMC3* variant T cells showed reduced expression of the PSMC3/Rpt5 full-length protein, suggesting that proteasome dysfunction in these affected individuals was not caused by haploinsufficiency.

Next, T cells from affected individuals and relative controls were analyzed for proteasome complex formation and activity by in-gel fluorescence followed by Western blotting on native-PAGE. As shown in Fig. 4B, the chymotrypsin-like activity of the 26S and 20S proteasome complexes (LLVY-AMC) was reduced for the majority of comparisons between patients and controls. Subsequent Western-blot analysis revealed that the decreased 20S activity observed in Patient #21 was associated with a decreased pool of 20S-PA28 complexes, as determined by reduced band intensity for the $\alpha 6$ and PA28 proteins. The amounts of unbound PA28 α/β complexes in T cells were increased in Patient #13 and decreased in Patient #18 (Fig. 4B). The reasons for these contrasting data between these two patients are unclear but might reflect distinct abilities to compensate for proteasome dysfunction. It should be noted, however, that, in contrast to PA28-bound proteasomes whose amounts did not change in these patients, free PA28 α/β are not equipped with

protease activity and as such have no impact on intracellular proteolysis. Densitometric analysis of the PSMC3/Rpt5 signals revealed impaired subunit incorporation into 26S, hybrid and 30S proteasome complexes in patients when compared to controls ($P=0.0329$) (Fig. 4B, bottom). Diminished expression of the $\alpha 6$ and PSMC3/Rpt5 subunits was observed in the 26S proteasomes of Patient #18 (Fig. 4B), indicating that the decline in 26S activity detected in this patient was likely to be attributed to decreased amounts of 26S complexes. Likewise, the PSMC3/Rpt5 contents in 26S complexes were also reduced in Patient #21 (Fig. 4B). Unexpectedly 20S and 26S proteasome pools of Patient #13 did not substantially vary when compared to those of the related control (Fig. 4B). The minor effects exerted by the G262R substitution in Patient #13 may be partially explained by the fact that G262 is surrounded by a large amount of empty space (Fig. S11), thereby allowing this region of the PSMC3/Rpt5 protein to accommodate mutations to some extent. Nevertheless, these data indicated that both of the R304W and E305D PSMC3/Rpt5 variants affect 20S proteasome assembly, 26S proteasome assembly, or both in individuals with NDD/ID, whereas the G262R variant has little impact in this process (Table 1).

Quantitative proteomics identifies cellular pathways affected by *PSMC3* loss-of-function in patients with NDD/ID

To better understand the cellular consequences of *PSMC3* loss-of-function, we next performed a mass spectrometry-based comparative analysis of the T-cell proteomes of Patient #17 and Patient #21 (R304W and E305D, respectively) to that of their relative controls. As shown in Fig. 5, our data identified a protein signature consisting of seventeen ribosomal proteins of the small 40S (RPS) or large 60S (RPL) ribosomal subunits that were specifically upregulated in both investigated patients. This suggests that mRNA translation is a major affected pathway upon *PSMC3* loss-of-function, a notion which is further supported by the fact that components of the mRNA processing machinery such as CUG-binding protein Elav-Like Family Member 1 (CELF1), a member of the LSM family of RNA-binding proteins (LSM1), RNA Polymerase II CTD Phosphatase (SSU72) and Inosine Triphosphatase (ITPA) were also differentially expressed between patients and controls (Fig. 5). Other notable proteins whose abundances varied in patients carrying *PSMC3* variants included components of the immune system such as MX Dynamin Like GTPase 1 (MX1) –a typical IFN-stimulated gene product– and the α -chain of the IL3 receptor (IL3RA). These proteins were regulated in opposite directions with both patients exhibiting higher amounts of MX1 but reduced amounts of IL3RA (Fig. 5). Our analysis further revealed that *PSMC3* loss-of-function was also associated with increased protein expression of the H1.5 and H1.2 linker histone H1 variants, a finding that is in line with a role of the UPS in chromatin regulation (46). Protein set enrichment analysis uncovered that most of the significant ($P<0.05$) proteomic changes between control and patients carrying *PSMC3* variants were related to mRNA metabolism and translation (Fig. S12), confirming that protein synthesis was dysregulated in these patients. Other differentially expressed proteins found to be enriched in T cells with *PSMC3* variants belonged to the category of viral processes (Fig. S12), unveiling a potential relationship between proteasome loss-of-function and innate immunity. Collectively, these data suggested that patients with *PSMC3* variants exhibit alterations in basic cellular processes including mRNA translation, immune signaling and chromatin remodeling.

***PSMC3* variants cause proteotoxic stress in patient T cells**

Proteasome dysfunction has been shown to be accompanied by accumulation of ubiquitin-protein conjugates and proteotoxic stress (24). As shown in Fig. 6A, all four investigated patients exhibited typical features of unbalanced protein homeostasis, as evidenced by increased accumulation of ubiquitin-modified species when compared to their respective related controls using immunoblotting and densitometric analysis. Proteotoxic stress is known to induce the unfolded protein response and integrated stress response (UPR and ISR, respectively) (24, 47). To address this point, we quantified the expression of the glucose-regulated protein 94 chaperone protein (GRP94, the heat shock protein 90kDa in the ER) whose upregulation is understood to be a major hallmark of the UPR (48). The expression of GRP94 was increased in all patients (Fig. 6A). However, the activation of the UPR was only partial, because the phosphorylation and activation status of two other UPR markers, namely serine/threonine-protein kinase/endoribonuclease inositol-requiring enzyme 1 α (IRE1) and eukaryotic translation initiation factor (eIF2) α , was not changed between controls and patients carrying *PSMC3* variants (Fig. 6A). The failure to detect increased phosphorylated eIF2 α , although the upstream kinase PKR was consistently activated in all patients (Fig. 6A), can be explained by upregulation of both eIF2 α phosphatases GADD34 (growth arrest and DNA damage-inducible protein 34) and CREP (constitutive repressor of eIF2 α phosphorylation) across all four patients. Immunoblotting and densitometric analysis revealed that T cells of the patients carrying *PSMC3* variants were also endowed with increased protein expression of microtubule-associated protein 1A/1B-light chain 3 phosphatidylethanolamine conjugate LC3b-II (Fig. 6B), suggesting that the inability of these cells to eliminate ubiquitin-protein aggregates cells via their 26S proteasomes triggers a compensatory mechanism mediated by activation of the autophagy system. Consistently, the mitochondrial proteins PINK1 (PTEN-induced putative kinase protein 1) and Bnip3L/NIX (BCL2/adenovirus E1B 19 kDa protein-interacting protein 3-like/NIP3-like protein X) were found to be decreased in the patients carrying *PSMC3* variants (Fig. 6B, Table 1), supporting the notion that selective autophagic processes including mitophagy were activated upon *PSMC3* disruption. Because proteasome impairment typically results in the release of the TCF11/Nrf1 (transcription factor 11/nuclear factor, erythroid derived 2, like 1) protein from the ER membrane (49, 50), we next sought to determine the TCF11/Nrf1 processing pattern in NDD/ID affected individuals. However, no differences in the TCF11/Nrf1 processing pattern could be detected between controls and patients carrying *PSMC3* variants (Fig. 6B), suggesting that *PSMC3* variants associated with NDD/ID do not lead to activation of the TCF11/Nrf1 signaling pathway.

T cells with *PSMC3* variants exhibit a type I IFN signature

Because proteasome loss-of-function results in the generation of a typical type I IFN response in PRAAS patients (30), we next sought to determine whether alterations in the *PSMC3* gene would induce type I IFN signatures as well. To this end, we undertook a comparative examination of the mRNA expression of 750 predefined immunologically relevant genes in T cells from patients carrying *PSMC3* variants and relative controls (father and/or mother) using the NanoString[®] nCounter platform. A total of 30 differentially expressed genes could be identified including 11 IFN-stimulated genes (ISGs) that were specifically upregulated in all patients carrying *PSMC3* variants (Fig. 7A), suggesting

that *PSMC3* loss-of-function is associated with type I IFN responses. The transcriptomic analysis of control and patient T cells further revealed that *PSMC3* disruption resulted in the upregulation of genes of the notch signaling pathway such as NOTCH2 (neurogenic locus notch homolog protein 2) and JAG2 (protein jagged-2) involved in developmental pathways including neurodevelopment (51) (Fig. 7A). To validate the type I IFN gene signature revealed by our omics profiling, we next evaluated the expression of seven ISG (*IFI27*, *IFI44L*, *IFIT1*, *ISG15*, *MX1*, *RSAD2* and *IFI44*) in samples of these four families with *PSMC3* missense variants. As shown in Fig. 7B, all four affected children's samples (Patients #13, #17, #18 and #21) exhibited much higher ISG expression than their parents (father and/or mother; Table 1). Calculation of the fold change median of the seven ISG revealed that a significant increase was detected in all *PSMC3* index cases when compared to their respective controls (Patient #13 vs father, $p=0.0148$; Patient #17 vs mother, $p=0.0008$; Patient #18 vs father, $p=0.0002$, Patient #18 vs mother, $p=0.0011$; Patient #21 vs father, $p=0.0012$ and Patient #21 vs mother, $p=0.0142$) (Fig. 7B). The strongest type I IFN signature was observed in Patient #18 whose ISG were upregulated by approximately 40- or 10-fold when compared to the father or mother, respectively. Patients #13, #17 and #21 exhibited a milder type I IFN induction characterized by a 2-to 6-fold increase in ISG transcripts than their respective controls. Among the seven ISGs tested, *IFIT1*, and *IFI44L* were the genes which underwent the most pronounced upregulation in all four affected individuals.

The type I IFN signature generated in *PSMC3* mutant T cells is PKR-dependent

We next calculated and compared the IFN scores of both patients carrying *PSMC3* variants and their related controls to those of T cells isolated from six healthy donors. As shown in Fig. 8A, three of the related controls had an IFN score slightly above the cut-off value of 2.466 defined by Rice et al. to be abnormal (52). However, the IFN scores of all related and unrelated controls remained significantly lower than those of the four tested patients ($P=0.0845$ and $P=0.0044$), thereby confirming that these *PSMC3* variants were associated with enhanced type I IFN signaling. A second independent assessment of Patient #18 at 14 months after enrollment revealed that this patient still exhibited a very high type I IFN score (Fig. S13). Because all three inducible immunoproteasome subunits $\beta 1i$ (*PSMB9*), $\beta 2i$ (*PSMB10*) and $\beta 5i$ (*PSMB8*) are encoded by genes typically stimulated by type I and II IFN (20), we next asked whether *PSMC3* loss-of-function was accompanied by a switch from standard proteasomes to immunoproteasomes. As illustrated in Fig. S14, the steady-state expression of these subunits in T cells did not substantially change between control and patients, as determined by Western-blotting. This may be due to the known fact that T cells, as immune cells, express high amounts of immunoproteasomes, a feature that renders any further protein upregulation of the inducible subunits very difficult (53).

We next attempted to unravel the mechanisms by which type I IFN responses were initiated in patients carrying *PSMC3* loss-of-function variants. Having shown that all four affected patients exhibited marked alterations in the mitophagy, UPR and ISR pathways (Fig. 6), we postulated that the dysregulation of either one of these pathways might act as a danger signal triggering innate immunity. To address this point, we inhibited key players of the UPR and/or ISR including PKR, IRE1 and GADD34 (24) by treating patient T cells with

the C16, 4 μ 8C or Guanabenz inhibitors, respectively. In addition, the potential implication of mitophagy-mediated mitochondrial DNA in this process was investigated by treating the cells with H-151, an inhibitor of the cytosolic DNA sensor STING (stimulator of interferon genes protein) (54). Of the four inhibitors used, only C16, targeting PKR, could substantially reduce the type I IFN response associated with *PSMC3* variants in these patients (Fig. 8B). These data thus suggest PKR as a sensor of proteasome dysfunction triggering a type I IFN signature in individuals carrying *PSMC3* variants.

DISCUSSION

In this study, we identified fifteen missense variants in the *PSMC3* gene in twenty-three unrelated individuals with NDD/ID (Fig. 1, Tables 1 and S1) and showed that the 19S AAA-ATPase proteasome subunit PSMC3/Rpt5 is a critical protein for the development of the central nervous system (CNS). This notion is in line with previous reports showing that conditional inactivation of other 19S proteasome subunits (*Psmc2/Rpt2* and *Psmc4/Rpt3*) in mice results in severe neuronal phenotypes with features of neurodegeneration and locomotor dysfunction (55, 56). Recently, a homozygous deep intronic variant creating a cryptic exon in the *PSMC3* gene was linked to a familial recessive neurosensory syndrome (57). However, given their distinct modes of inheritance and pathogenesis, this recessive disorder observed in a single family and the dominant variants, which we describe are likely two different clinical entities with only partial overlap of clinical and molecular disease phenotypes (57). This dichotomy between dominant and recessive disorders may, nevertheless, be too reductive, because our data show that the dominant *PSMC3* variants do not necessarily exert the same effects on proteasome expression, assembly, or both (Figs. 3A, 4B and Table 1). These variations make it difficult to classify dominant *PSMC3* variants according to their impact on cellular function without any in vitro functional studies.

There are several limitations to this study. Given the limited number of biological samples investigated, a correlation between genotype and cellular phenotype could not be established. In this regard it should also be noted that the gene silencing in the *Drosophila* model does not completely reflect disease biology patients, given that gene product is still available. We can furthermore not fully exclude a recruitment bias in our patient data set.

Cognitive flexibility is an important aspect of typical brain function which allows adaptation to both physical and social environmental changes (58, 59). This may be assessed by evaluating reversal learning performance, a process which was initially identified in *Drosophila* models (60) and whose dysfunction has been associated with the pathogenesis of various neuropsychiatric disorders (61–65). Although Rpt5 gene-silencing in flies had no discernible effect on learning performance, it led to compromised reversal learning (Fig. 2). Although proteasomes have been shown to regulate long-term potentiation (LTP) (66, 67), their involvement in reversal learning has not previously been shown. Our data identify PSMC3/Rpt5 as a key regulator of this process whose molecular landscape was initially limited to a few molecules related to the cytoskeleton and GABAergic system (68–70). One cannot exclude that Rpt5 gene-silencing in *Drosophila* may result in global depletion of 26S complexes which in turn impairs reversal learning. However, some of the missense mutations identified in this study led to decreased PSMC3/Rpt5 expression

(Fig. 3A), reduced incorporation into 26S complexes (Fig. 4B), or both suggesting that a shortage of the PSMC3/Rpt5 subunit may indeed reflect disease pathogenesis. The mechanisms by which proteasomes regulate reversal learning are unclear but may imply the degradation of specific neuronal proteins to control some synaptic connections and “reset” learning associations. It is tempting to speculate that one of these substrates could be Arc (activity-regulated cytoskeleton-associated protein), a key mediator of synaptic plasticity whose persistent expression has recently been shown to interfere with the reversal learning process (71). Additional evidence in favour of a critical role of PSMC3/Rpt5 in behavioural flexibility emerged from our experiments in primary hippocampal neurons showing that ectopic expression of PSMC3/Rpt5 affected dendrite growth (Fig. S3). The observation that the R304W, E305D and E383L *PSMC3* variants did not differ from their wild-type counterpart in this process is intriguing but may have several explanations. First, wild-type *PSMC3* overexpression may exert ceiling effects that overshadow any potential detrimental impact of the *PSMC3* variants on neuronal morphology. Secondly, it may be that *PSMC3* variants, with the exception of M159V, have no substantial effect on neuronal morphology. The reasons why the M159V *PSMC3* variant behaves differently are unclear but these findings might be explained by distinct half-life, intracellular localization or post-translational modifications. One could also argue that the adverse effects of PSMC3/Rpt5 on this process might be due to extra-proteasome functions as a consequence of an excess of “free” subunits following transfection. However, our investigations on patient T cells showed that *PSMC3* missense variants were associated with an increased accumulation of ubiquitin-modified proteins (Fig. 6A), suggesting that these alterations give rise to proteasome loss-of-function variants associated with perturbed protein homeostasis. Future functional studies involving a larger number of biological samples are required to evaluate a possible correlation between *PSMC3* variants and the extent of intracellular proteolysis dysfunction as a prerequisite for predicting disease severity.

Our proteomic analysis revealed that T cells from patients carrying *PSMC3* variants were enriched with ribosomal proteins such as RPL4, RPL6, RPL7A and RPL7 (Fig. 5 and Table 2). These proteins may be specifically targeted for degradation and their accumulation may occur as a consequence of impaired intracellular protein clearance. Consistent with this notion, proteasome inhibition has been recently shown to result in the aggregation of ubiquitin-modified ribosomal proteins (72). Our data therefore support the recent view that ribosome dysregulation defines a key feature of NDD/ID phenotypes (73, 74) and the concept of translational arrest upon proteotoxic stress via the action of eIF2 α kinases (Fig. 6A).

One key finding is the observation that patients with *PSMC3* variants generate a type I IFN gene signature (Figs. 7 and 8A). Although it is well-established that proteasome loss-of-function variants cause interferonopathies in patients with PRAAS (27–33), it was only recently that pathogenic mutations in the 19S regulatory particle subunit PSMD12/Rpn5 were reported to engage constitutive type I IFN signaling in patients with this NDD disorder (35, 36) sharing similarities with the patients described in this manuscript. Although patients with PRAAS and individuals with NDD/ID and *PSMD12* or *PSMC3* variants carry genomic alterations that affect the same multi-subunit enzyme (26S proteasome), their clinical phenotypes do not entirely overlap. For instance, patients with NDD/ID and *PSMC3* variants

did not develop recurrent fever, lipodystrophy and/or skin lesions which are usually detected in patients with PRAAS (Table 1). One could argue that such differences may reflect distinct localizations of the affected subunits within the 26S proteasome complex, thereby suggesting that alterations of the 19S regulatory particle promote the generation of NDD/ID, whereas those of the 20S core particle or assembly chaperones favor the development a PRAAS phenotype. This assumption is however challenged by the fact that PSMB1/ β 6 variants of the 20S core particle lead to the acquisition of neuronal phenotype very similar to that observed in patients with NDD/ID and *PSMC3* variants (25). The lack of systemic autoinflammation in patients with NDD/ID and *PSMC3* variants mounting a constitutive type I IFN response may seem surprising at first sight, but it is not totally unexpected, since this inconsistency is found in other NDDs including Aicardi-Goutières (75, 76) and Down syndromes (77, 78). This is particularly well exemplified in Down syndrome patients who, like patients with NDD/ID and *PSMC3* dominant variants, exhibit a constitutive activation of type I IFN signaling (79, 80). To what extent type I IFN actively contributes to the pathogenesis of these disorders remains to be fully determined, even though a growing body of evidence supports the notion that IFN has detrimental effects on CNS function (81–84) as well as stem cell function and differentiation (85, 86). Because proteasome dysfunction typically engages stress responses involving compensatory mechanisms such as autophagy (87), ISR and UPR (24, 88), we reasoned that the type I IFN response detected in patients with *PSMC3* variants might be triggered by sustained activation of either one of these pathways. As anticipated, high expression of autophagy and ER stress markers were detected in affected individuals, as evidenced by increased expression of the LC3-II and GRP94 proteins (Fig. 6A and B). Both PINK1 and NIX mitochondrial proteins were found to be decreased in affected individuals (Fig. 6B), suggesting that *PSMC3* variants increase autophagy-driven elimination of mitochondria (mitophagy). This observation supports the growing consensus that mitochondrial dysfunction is a key determinant of the pathogenesis of neurodevelopment (89) and the cause of interferonopathies (90). The activation status of PKR, a protein of the ISR that intersects with the UPR (91), was substantially increased in all investigated patients carrying the *PSMC3* variant. Both ISR and UPR have the ability to counterbalance proteotoxic stress by inducing a global translational arrest via eIF2 α phosphorylation. This is accompanied by concomitant accumulation of non-translated mRNAs, the formation of stress granules recruiting different RNA species and RNA processing enzymes, and IRE-1-dependent mRNA decay (RIDD) (92). Although PKR typically responds to viral double stranded RNA (93), it also may undergo activation under sterile conditions upon different stresses including ER-stress involving PKR-associated activator (PACT) and its modulator TAR RNA-binding protein 2 (TRBP), a protein required for micro-RNA biogenesis (94–96). Both PACT and TRBP were observed to be increased in patient cells along with several RNA-processing factors. Our inhibition experiments suggested PKR as the inducer of type I IFN in these patients (Fig. 8B). The mechanisms by which *PSMC3* variants activate PKR in affected individuals remain unclear, but our data open the possibility that PKR may sense a broader spectrum of danger signals than initially assumed, including perturbations of protein homeostasis. This concept is in line with the observation that activated PKR was found in the CNS of patients with neurodegenerative diseases (97–100) and that neurodegeneration is associated with neuroinflammation (101, 102). Altogether, our work demonstrates that heterozygous *PSMC3* dominant variants result

in a neurodevelopmental syndrome associated with a specific type I IFN gene signature and suggests treatment options targeting type I IFN signaling or PKR.

MATERIALS AND METHODS

Study design

The aim of the study was to determine the involvement of the human *PSMC3* gene in a neurodevelopmental disorder hitherto unreported. Affected individuals were recruited and data were collected on an ongoing basis. Affected individuals were identified via data sharing platform GeneMatcher (103) and direct requests in variants databases whose access was authorized to the University of Washington School of Medicine. Clinical and molecular data were provided by the referring geneticists following the patients. Facial recognition by GestaltMatcher (41) was used to measure the similarities of the facial phenotypes between affected individuals (Fig. S2). Prediction of variant pathogenicity was done using the bioinformatics programs indicated in Table 1, and their frequency was determined in public variant databases (gnomAD (104), Exome Variant Server, NHLBI GO Exome Sequencing Project (ESP), Seattle, WA (URL: <http://evs.gs.washington.edu/EVS/>) [03/2023 accessed]; Bravo powered by TOPMed Freeze 8 on GRCh38 (105)). The effects of the *PSMC3* variants on proteasome function, protein homeostasis, proteotoxic stress sensors (UPR, ISR), autophagy/mitophagy and inflammation status (type I IFN) were studied *in vitro* by western-blotting, NanoString® analysis and qPCR using T cells expanded from whole-blood samples of patients (n=4) and their parents (n=6) who agreed to provide blood specimens. The first available T-cell samples (patients n=2, related controls n=2) were used for proteomics analyses to explore deregulated biological pathways. The impact of the variants on neuronal function was assessed in two models: 1. Upstream Activation Sequence (UAS)-Rpt5 RNAi *Drosophila melanogaster* lines targeting *psmc3* for evaluating the effect of Rpt5 knockdown on behavior (Fig. 2); 2. primary hippocampal neuronal cultures overexpressing cDNA constructs containing the first identified variants (n=4) for evaluating their effects on neuronal morphology (Fig. S3). Details about data replication are provided in the figure legends. Experimenters were not blinded.

Human participants

All affected participants were initially referred for unexplained developmental delay (DD) and/or intellectual disability (ID) together with various congenital malformations. They underwent extensive clinical examination by at least one clinical geneticist participating in the study. Routine genetic testing was performed whenever clinically relevant, including copy number variation (CNV) analysis by high-resolution array-based comparative genomic hybridization (aCGH). Because these tests failed to establish the diagnosis of a specific disease, trio-based whole exome sequencing (WES) was performed on a diagnostic or research setting whenever parental samples were available. Because disorders associated with *PSMC3* are very rare, the reported patient cohort is representative of cases identified worldwide over the past six years and is not, for example, a selection of a subgroup of a larger patient population. This study was approved by the CHU de Nantes ethics committee (Research Programme “Génétique Médicale DC-2011–1399). Probands 2, 5–10, 12–14, 16–18, and 20–23 were enrolled by one of the participating centers (Washington University in

St. Louis, University Medical Centre of Utrecht, University Hospital Center of Nantes, Arnold Palmer Hospital, Seattle Children's Hospital, St. Luke's Hospital, Health San Antonio, Vanderbilt University Medical Center, Sydney Medical School, Children's Hospital of Philadelphia, Technical University of Munich, Pitié-Salpêtrière University Hospital, Children's Hospital of Orange County, Ambry Genetics, Geisinger Medical Center, Guy's & St Thomas' NHS Foundation Trust, McGill University Health Centre, Nottingham University Hospitals NHS Trust, Hôpital Universitaire Necker-Enfants Malades, University Children's Hospital, Salzburger Landeskliniken (SALK) and Paracelsus Medical University) after approval of genetic studies by local ethics committees. Written informed consent was obtained from all study participants, including probands and healthy parents. All affected individuals were initially referred for unexplained developmental delay (DD) and/or intellectual disability (ID) together with various congenital malformations. They underwent extensive clinical examination by at least one expert clinical geneticist. Individuals 1, 4, 11, 15 and 19 participated in 'Simons Foundation Powering Autism Research' (SPARK) or 'Deciphering Developmental Disorders' initiative; clinical information about individuals 1, 3 and 14 was retrieved by members of the University of Washington School of Medicine in agreement with SPARK and DDD.

Cell culture

Peripheral blood mononuclear cells (PBMC) used in this paper were isolated from blood draws from patients and related healthy controls (father and/or mother of the proband). Briefly, PBMC were isolated by PBMC spin medium gradient centrifugations (pluriSelect), washed three times with PBS, frozen in FBS with 10% DMSO and stored in liquid nitrogen for further use. In some experiments, collected PBMC were expanded in U-bottom 96-well plates together with feeder cells using RPMI 1640 supplemented with 10% human AB serum (both purchased from PAN-Biotech GmbH) in the presence of 150 U/ml IL-2 (Miltenyi Biotec) and 1 µg/µl L-PHA (Sigma) following the procedure of Fonteneau et al. (106). After 3–4 weeks of culture, resting T cells were washed and frozen as dry pellets for further use.

SDS-PAGE and western-blot analysis

Cell pellets from resting T cell isolated from patients and related controls were lysed in equal amounts of standard RIPA buffer (50 mM Tris pH 7.5, 150 mM NaCl, 2 mM EDTA, 1 mM N-ethylmaleimide, 10 µM MG-132, 1% NP40, 0.1% SDS) and separated by 10 or 12.5% SDS-PAGE before transfer to PVDF membranes (200V for 1h). After blocking (20-min exposure to 1X Roti®-Block at room temperature), membranes were probed with relevant primary antibodies overnight at 4°C under shaking. The anti-α6 (clone MCP20), anti-α7 (clone MCP72), anti-β1 (clone MCP421), anti-PSMC2 (BML-PW8315) and anti-PSMC3 (BML-PW8310) primary antibodies were purchased from Enzo Life Sciences. Primary antibodies specific for TCF11/Nrf1 (clone D5B10), ubiquitin (clone D9D5), GAPDH (clone 14C10), PINK1 (clone D8G3), BNIP3L/NIX (clone D8G3), LC3b (#2775), eIF2α (#9722), phospho-eIF2α (ser51, #119A11) were obtained from Cell Signaling Technology. The anti-PSMD12 antibody (clone H3) was a purchase from Santa Cruz Biotechnology Inc. The anti-PA28-α (K232/1) is laboratory stock and was used in previous studies (31). Antibodies directed against β5 (ab33330), α-Tubulin (clone DM1A)

and phospho-PKR (Thr446, clone E120) were purchased from Abcam. Following incubation with primary antibodies, membranes were washed three times with PBS/0.2% Tween and subsequently incubated with anti-mouse or –rabbit HRP conjugated secondary antibodies (1/5.000) for 1h at room temperature. Proteins were then visualized using an enhanced chemiluminescence detection kit (ECL) (Biorad).

RNA isolation, reverse-transcription and PCR analysis

Total RNA was isolated from resting T cells using the kit from Analytic Jena AG following the manufacturer's instructions. For subsequent real-time PCR, 100–500 ng of the isolated total RNA was reverse transcribed using the M-MLV reverse transcriptase (Promega). Quantitative PCR was performed using the Premix Ex Taq™ (probe qPCR purchased from TaKaRa) and in duplicates to determine the mRNA expression of each IFN-stimulated gene (ISG) using FAM-tagged TaqMan™ Gene Expression Assays obtained from Thermo Fisher Scientific according to the manufacturer's instructions. TaqMan™ probes used in this study for ISG quantification included *IFI27*, *IFI44L*, *IFIT1*, *ISG15*, *RSAD2*, *IFI44*, *MX1*, *OASL1*, *CXCL9* and *CXCL10*. The cycle threshold (Ct) values for target genes were converted to values of relative expression using the relative quantification (RQ) method (2^{-Ct}). Target gene expression was calculated relative to Ct values for the GAPDH control housekeeping gene.

Statistical analyses

Figures were created with PyMOL v. 2.0 (pymol.org) using the human 26S proteasome structure. Data are typically median or mean \pm SEM and analyzed by unpaired and pair ratio t-test between two groups. Neuronal morphology data was analyzed using a One-Way analysis of variance (ANOVA), followed by a Tukey's post-hoc test for multiple comparisons. All charts and statistical analyses were generated using GraphPad Prism version 8. A p-value <0.05 was considered significant.

Supplementary Material

Refer to Web version on PubMed Central for supplementary material.

Authors

Frédéric Ebstein^{1,†}, Sébastien Küry^{2,3,†}, Victoria Most⁴, Cory Rosenfelt⁵, Marie-Pier Scott-Boyer⁶, Geeske M. van Woerden^{7,8,9}, Thomas Besnard^{2,3}, Jonas Johannes Papendorf¹, Maja Studencka-Turski¹, Tianyun Wang^{10,11,12}, Tzung-Chien Hsieh¹³, Richard Golnik¹⁴, Dustin Baldrige¹⁵, Cara Forster¹⁶, Charlotte de Konink^{7,8}, Selina M.W. Teurlings^{7,8}, Virginie Vignard^{2,3}, Richard H. van Jaarsveld¹⁷, Lesley Ades^{18,19}, Benjamin Cogné^{2,3}, Cyril Mignot^{20,21}, Wallid Deb^{2,3}, Marjolijn C.J. Jongmans^{17,22}, F. Sessions Cole¹⁵, Marie-José H. van den Boogaard¹⁷, Jennifer A. Wambach¹⁵, Daniel J. Wegner¹⁵, Sandra Yang¹⁶, Vickie Hannig²³, Jennifer Ann Brault²³, Neda Zadeh²⁴, Bruce Bennetts^{19,25}, Boris Keren²⁶, Anne-Claire Gélinau²⁶, Zöe Powis²⁷, Meghan Towne²⁷, Kristine Bachman²⁸, Andrea Seeley²⁸, Anita E. Beck²⁹, Jennifer Morrison³⁰, Rachel Westman³¹, Kelly Averill³², Theresa Brunet^{33,34}, Judith

Haasters³⁵, Melissa T. Carter^{36,37}, Matthew Osmond³⁶, Patricia G. Wheeler³⁰, Francesca Forzano^{38,39}, Shehla Mohammed^{38,39}, Yannis Trakadis⁴⁰, Andrea Accogli⁴⁰, Rachel Harrison^{38,41}, Yiran Guo^{42,43}, Hakon Hakonarson⁴², Sophie Rondeau⁴⁴, Geneviève Baujat⁴⁴, Giulia Barcia⁴⁴, René Günther Feichtinger⁴⁵, Johannes Adalbert Mayr⁴⁵, Martin Preisel⁴⁵, Frédéric Laumonier^{46,47}, Tilmann Kallinich^{48,49}, Alexej Knaus¹³, Bertrand Isidor^{2,3}, Peter Krawitz¹³, Uwe Völker⁵⁰, Elke Hammer⁵⁰, Arnaud Droit⁶, Evan E. Eichler^{10,51}, Ype Elgersma^{8,9}, Peter W. Hildebrand^{4,52,53}, François Bolduc^{5,54,55,‡}, Elke Krüger^{1,‡,*}, Stéphane Bézieau^{2,3,‡,*}

Affiliations

¹Institut für Medizinische Biochemie und Molekularbiologie (IMBM),
Universitätsmedizin Greifswald, Ferdinand-Sauerbruch-Straße, 17475 Greifswald,
Germany

²Nantes Université, CHU Nantes, Service de Génétique Médicale, 44000 Nantes,
France

³Nantes Université, CHU Nantes, CNRS, INSERM, l'institut du thorax, 44000
Nantes, France

⁴Institut für Medizinische Physik und Biophysik, Universität Leipzig, Medizinische
Fakultät, Härtelstr. 16-18, 04107 Leipzig, Germany

⁵Department of Pediatrics, University of Alberta, Edmonton, AB CT6G 1C9, Canada

⁶Research Center of Quebec CHU-Université Laval, Québec, QC PQ G1E6W2,
Canada

⁷Department of Neuroscience, Erasmus University Medical Center, 3015 CN,
Rotterdam, The Netherlands

⁸ENCORE Expertise Center for Neurodevelopmental Disorders, Erasmus University
Medical Center, 3015 CN, Rotterdam, The Netherlands

⁹Department of Clinical Genetics, Erasmus University Medical Center, 3015 CN,
Rotterdam, The Netherlands

¹⁰Department of Genome Sciences, University of Washington School of Medicine,
Seattle, WA 98195, USA

¹¹Department of Medical Genetics, Center for Medical Genetics, School of Basic
Medical Sciences, Peking University Health Science Center, Beijing 100191, China

¹²Neuroscience Research Institute, Peking University; Key Laboratory for
Neuroscience, Ministry of Education of China & National Health Commission of
China, Beijing 100191, China

¹³Institute for Genomic Statistics and Bioinformatics, University Hospital Bonn,
Rheinische Friedrich-Wilhelms-Universität Bonn, 53127 Bonn, Germany

¹⁴Klinik für Pädiatrie I, Universitätsklinikum Halle (Saale), 06120 Halle (Saale)

¹⁵The Edward Mallinckrodt Department of Pediatrics, Washington University School of Medicine, St. Louis, MO 63130-4899, USA

¹⁶GeneDx, 207 Perry Parkway, Gaithersburg, MD 20877, USA

¹⁷Department of Genetics, University Medical Center Utrecht, 3508 AB, Utrecht, The Netherlands

¹⁸Department of Clinical Genetics, The Children's Hospital at Westmead, Locked Bag 4001, Westmead, NSW, 2145, Australia

¹⁹Disciplines of Genomic Medicine & Child and Adolescent Health, Faculty of Medicine and Health, University of Sydney, Sydney, NSW, 2145, Australia

²⁰APHP, Hôpital Pitié-Salpêtrière, Département de Génétique, Centre de Référence Déficience Intellectuelle de Causes Rares, GRC UPMC «Déficience Intellectuelle et Autisme», 75013 Paris, France

²¹Sorbonne Universités, Institut du Cerveau et de la Moelle épinière, ICM, Inserm U1127, CNRS UMR 7225, 75013, Paris, France

²²Princess Máxima Center for Pediatric Oncology, 3584 CS, Utrecht, The Netherlands

²³Department of Medicine, Vanderbilt University Medical Center, Nashville, TN 37232, USA

²⁴Genetics Center, Orange, CA 92868, USA; Division of Medical Genetics, Children's Hospital of Orange County, Orange, CA 92868, USA

²⁵Sydney Genome Diagnostics, Western Sydney Genetics Program, The Children's Hospital at Westmead, Sydney, NSW, 2145, Australia

²⁶Département de Génétique, Centre de Référence des Déficiences Intellectuelles de Causes Rares, Groupe Hospitalier Pitié-Salpêtrière, Assistance Publique-Hôpitaux de Paris, 75013 Paris

²⁷Department of Clinical Research, Ambry Genetics, Aliso Viejo, CA 92656, USA

²⁸Genomic Medicine Institute, Geisinger, Danville, PA 17822, USA

²⁹Department of Pediatrics, Division of Genetic Medicine, University of Washington & Seattle Children's Hospital, Seattle, WA 98195-6320, USA

³⁰Division of Genetics, Arnold Palmer Hospital for Children, Orlando Health, Orlando, FL 32806, USA

³¹Division of Genetics, St. Luke's Clinic, Boise, ID 83712, USA

³²Department of Pediatrics, Division of Pediatric Neurology, UT Health Science Center at San Antonio, San Antonio, TX 78229, USA

³³Institute of Human Genetics, Technical University of Munich, School of Medicine, 81675 Munich, Germany

- ³⁴Institute of Neurogenomics (ING), Helmholtz Zentrum München, German Research Center for Environmental Health, 85764 Neuherberg, Germany
- ³⁵Klinikum der Universität München, Integriertes Sozial- pädiatrisches Zentrum, 80337 Munich, Germany
- ³⁶Children's Hospital of Eastern Ontario Research Institute, University of Ottawa, ON K1H 8L1, Canada
- ³⁷Department of Genetics, Children's Hospital of Eastern Ontario, Ottawa, ON K1H 8L1, Canada
- ³⁸Wellcome Trust Sanger Institute, Wellcome Trust Genome Campus, Hinxton, Cambridge CB10 1SA, UK
- ³⁹Clinical Genetics Department, Guy's & St Thomas' NHS Foundation Trust, London SE1 9RT, UK
- ⁴⁰Division of Medical Genetics, McGill University Health Centre, Montreal, QC H4A 3J1, Canada
- ⁴¹Department of Clinical Genetics, Nottingham University Hospitals NHS Trust, City Hospital Campus, The Gables, Gate 3, Hucknall Road, Nottingham NG5 1PB, UK
- ⁴²Center for Applied Genomics, Children's Hospital of Philadelphia, Philadelphia, PA 19104, USA
- ⁴³Center for Data Driven Discovery in Biomedicine, Children's Hospital of Philadelphia, Philadelphia, PA 19146, USA
- ⁴⁴Service de Médecine Génomique des Maladies Rares, Hôpital Universitaire Necker-Enfants Malades, 75743 Paris, France
- ⁴⁵University Children's Hospital, Salzburger Landeskliniken (SALK) and Paracelsus Medical University (PMU), 5020 Salzburg, Austria
- ⁴⁶UMR 1253, iBrain, Université de Tours, Inserm, 37032 Tours, France
- ⁴⁷Service de Génétique, Centre Hospitalier Régional Universitaire, 37032 Tours, France
- ⁴⁸Department of Pediatric Respiratory Medicine, Immunology and Critical Care Medicine, Charité Universitätsmedizin Berlin; 13353 Berlin, Germany
- ⁴⁹Deutsches Rheumaforschungszentrum, An Institute of the Leibniz Association, Berlin and Berlin Institute of Health, 10117 Berlin, Germany
- ⁵⁰Universitätsmedizin Greifswald, Interfakultäres Institut für Genetik und Funktionelle Genomforschung, Abteilung für Funktionelle Genomforschung, 17487 Greifswald, Germany
- ⁵¹Howard Hughes Medical Institute, University of Washington, Seattle, WA, 98195, USA

⁵²Charité Universitätsmedizin Berlin, corporate member of Freie Universität Berlin and Humboldt-Universität zu Berlin, Institute of Medical Physics and Biophysics, Berlin, Germany

⁵³Berlin Institute of Health, 10178 Berlin, Germany

⁵⁴Neuroscience and Mental Health Institute, University of Alberta, Edmonton, AB T6G 2E1, Canada

⁵⁵Department of Medical Genetics, University of Alberta, Edmonton, AB T6G 2H7, Canada

Acknowledgments:

The sequencing for Patient #3 was performed under the Care4Rare Canada Consortium funded by Genome Canada and the Ontario Genomics Institute (OGI-147), the Canadian Institutes of Health Research, Ontario Research Fund, Genome Alberta, Genome British Columbia, Genome Quebec, and Children's Hospital of Eastern Ontario Foundation. The Deciphering Developmental Disorder (DDD) study presents independent research commissioned by the Health Innovation Challenge Fund [grant number HICF-1009-003]. This study makes use of DECIPHER (<http://www.deciphergenomics.org>), which is funded by the Wellcome Trust. The authors are grateful to R. Beyer and A. Brandenburg for excellent technical assistance.

Funding:

This work was supported by German Research Foundation Grants SFBTR167, RGT2719-PRO project B4 (to EK), E-Rare project GENOMIT (Austrian Science Fund FWF, I4695-B) to JAM, US National Institutes of Health (NIH) grants (R01MH101221) and a grant from the Simons Foundation (SFARI #608045) to EEE. EEE is an investigator of the Howard Hughes Medical Institute. This work was also supported, in part, by "the Fundamental Research Funds for the Central Universities" starting fund (BMU2022RCZX038) to TW.

References and notes

1. Tanaka K, Mizushima T, Saeki Y. The proteasome: molecular machinery and pathophysiological roles. *Biol Chem* 393, 217–34 (2012). [PubMed: 23029643]
2. Collins GA, Goldberg AL. The Logic of the 26S Proteasome. *Cell* 169, 792–806 (2017). [PubMed: 28525752]
3. Hetzer MW, Toyama BH, Protein homeostasis: live long, won't prosper. *Nat Rev Mol Cell Biol* 14, 55–61 (2013). [PubMed: 23258296]
4. Goloubinoff P. Mechanisms of protein homeostasis in health, aging and disease. *Swiss Med Wkly* 146, w14306 (2016). [PubMed: 27045704]
5. Seifert U, Bialy LP, Ebstein F, Bech-Otschir D, Voigt A, Schröter F, Prozorovski T, Lange N, Steffen J, Rieger M, Kuckelkorn U, Aktas O, Kloetzel P-M, Krüger E. Immunoproteasomes preserve protein homeostasis upon interferon-induced oxidative stress. *Cell* 142, 613–24 (2010). [PubMed: 20723761]
6. Krüger E, Kloetzel PM. Immunoproteasomes at the interface of innate and adaptive immune responses: Two faces of one enzyme. *Curr Opin Immunol* 24, 77–83 (2012). [PubMed: 22296715]
7. Pickart CM. Mechanisms underlying ubiquitination. *Annu Rev Biochem* 70, 503–33 (2001). [PubMed: 11395416]
8. DeMartino GN, Gillette TG. Proteasomes: Machines for All Reasons. *Cell* 129, 659–62 (2007). [PubMed: 17512401]
9. Pickart CM, Fushman D. Polyubiquitin chains: Polymeric protein signals. *Curr Opin Chem Biol* 8, 610–6 (2004). [PubMed: 15556404]
10. Pickart CM. Back to the Future with Ubiquitin. *Cell* 116, 181–90 (2004). [PubMed: 14744430]
11. Tanaka K. The proteasome: Overview of structure and functions. *Proc Jpn Acad Ser B Phys Biol Sci* 85, 12–36 (2009).

12. Dahlmann B. Mammalian proteasome subtypes: Their diversity in structure and function. *Arch Biochem Biophys* 591, 132–40 (2016). [PubMed: 26724758]
13. Tomko RJ, Funakoshi M, Schneider K, Wang J, Hochstrasser M. Heterohexameric Ring Arrangement of the Eukaryotic Proteasomal ATPases: Implications for Proteasome Structure and Assembly. *Mol Cell* 38, 393–403 (2010). [PubMed: 20471945]
14. Smith DM, Chang SC, Park S, Finley D, Cheng Y, Goldberg AL. Docking of the Proteasomal ATPases' Carboxyl Termini in the 20S Proteasome's α Ring Opens the Gate for Substrate Entry. *Mol Cell* 27, 731–44 (2007). [PubMed: 17803938]
15. Greene ER, Dong KC, Martin A. Understanding the 26S proteasome molecular machine from a structural and conformational dynamics perspective. *Curr Opin Struct Biol* 61, 33–41 (2020). [PubMed: 31783300]
16. Greene ER, Goodall EA, de La Peña AH, Matyskiela ME, Lander GC, Martin A. Specific lid-1 base contacts in the 26S proteasome control the conformational switching required for substrate degradation. *Elife* 8, e49806 (2019). [PubMed: 31778111]
17. Verma R, Aravind L, Oania R, McDonald WH, Yates JR, Koonin E. v., Deshaies RJ. Role of Rpn11 metalloprotease in deubiquitination and degradation by the 26S proteasome. *Science* 298, 611–615 (2002). [PubMed: 12183636]
18. Kisselev AF, van der Linden WA, Overkleeft HS. Proteasome inhibitors: An expanding army attacking a unique target. *Chem Biol* 19, 99–115 (2012). [PubMed: 22284358]
19. Finley D, Chen X, Walters KJ. Gates, Channels, and Switches: Elements of the Proteasome Machine. *Trends Biochem Sci* 41, 77–93 (2016). [PubMed: 26643069]
20. Ebstein F, Kloetzel P-M, Krüger E, Seifert U. Emerging roles of immunoproteasomes beyond MHC class I antigen processing. *Cell Mol Life Sci* 69, 2543–58 (2012). [PubMed: 22382925]
21. Strehl B, Seifert U, Krüger E, Heink S, Kuckelkorn U, Kloetzel PM. Interferon- γ , the functional plasticity of the ubiquitin-proteasome system, and MHC class I antigen processing. *Immunol Rev* 207, 19–30 (2005). [PubMed: 16181324]
22. Shin EC, Seifert U, Urban S, Truong KT, Feinstone SM, Rice CM, Kloetzel PM, Rehermann B. Proteasome activator and antigen-processing aminopeptidases are regulated by virus-induced type I interferon in the hepatitis C virus-infected liver. *J Interferon Cytokine Res* 27, 985–90 (2007). [PubMed: 18184038]
23. Brehm A, Krüger E. Dysfunction in protein clearance by the proteasome: impact on autoinflammatory diseases. *Semin Immunopathol* 37, 323–333 (2015). [PubMed: 25963519]
24. Ebstein F, Poli Harlowe MC, Studencka-Turski M, Krüger E. Contribution of the Unfolded Protein Response (UPR) to the Pathogenesis of Proteasome-Associated Autoinflammatory Syndromes (PRAAS). *Front Immunol* 10, 2756 (2019). [PubMed: 31827472]
25. Ansar M, Ebstein F, Özkoç H, Paracha SA, Iwaszkiewicz J, Gesemann M, Zoete V, Ranza E, Santoni FA, Sarwar MT, Ahmed J, Krüger E, Bachmann-Gagescu R, Antonarakis SE. Biallelic variants in PSMB1 encoding the proteasome subunit $\beta 6$ cause impairment of proteasome function, microcephaly, intellectual disability, developmental delay and short stature. *Hum Mol Genet* 29, 1132–1143 (2021).
26. Agarwal AK, Xing C, Demartino GN, Mizrachi D, Hernandez MD, Sousa AB, Martínez De Villarreal L, dos Santos HG, Garg A. PSMB8 Encoding the $\beta 5i$ Proteasome Subunit Is Mutated in Joint Contractures, Muscle Atrophy, Microcytic Anemia, and Panniculitis-Induced Lipodystrophy Syndrome. *Am J Hum Genet* 87, 866–72 (2010). [PubMed: 21129723]
27. Arima K, Kinoshita A, Mishima H, Kanazawa N, Kaneko T, Mizushima T, Ichinose K, Nakamura H, Tsujino A, Kawakami A, Matsunaka M, Kasagi S, Kawano S, Kumagai S, Ohmura K, Mimori T, Hirano M, Ueno S, Tanaka K, Tanaka M, Toyoshima I, Sugino H, Yamakawa A, Tanaka K, Niikawa N, Furukawa F, Murata S, Eguchi K, Ida H, Yoshiura KI. Proteasome assembly defect due to a proteasome subunit beta type 8 (PSMB8) mutation causes the autoinflammatory disorder, Nakajo-Nishimura syndrome. *Proc Natl Acad Sci U S A* 108, 14914–14919 (2011). [PubMed: 21852578]
28. Kitamura A, Maekawa Y, Uehara H, Izumi K, Kawachi I, Nishizawa M, Toyoshima Y, Takahashi H, Standley DM, Tanaka K, Hamazaki J, Murata S, Obara K, Toyoshima I, Yasutomo K. A

- mutation in the immunoproteasome subunit PSMB8 causes autoinflammation and lipodystrophy in humans. *J Clin Invest* 121, 4150–60 (2011). [PubMed: 21881205]
29. Liu Y, Ramot Y, Torreló A, Paller AS, Si N, Babay S, Kim PW, Sheikh A, Lee CCR, Chen Y, Vera A, Zhang X, Goldbach-Mansky R, Zlotogorski A. Mutations in PSMB8 Cause CANDLE Syndrome with Evidence of Genetic and Phenotypic Heterogeneity. *Arthritis Rheum* 64, 895–907 (2012). [PubMed: 21953331]
 30. Brehm A, Liu Y, Sheikh A, Marrero B, Omoyinmi E, Zhou Q, Montealegre G, Biancotto A, Reinhardt A, de Jesus AA, Pelletier M, Tsai WL, Remmers EF, Kardava L, Hill S, Kim H, Lachmann HJ, Megarbane A, Chae JJ, Brady J, Castillo RD, Brown D, Casano AV, Gao L, Chapelle D, Huang Y, Stone D, Chen Y, Sotzny F, Lee CCR, Kastner DL, Torreló A, Zlotogorski A, Moir S, Gadina M, McCoy P, Wesley R, Rother K, Hildebrand PW, Brogan P, Krüger E, Aksentijevich I, Goldbach-Mansky R. Additive loss-of-function proteasome subunit mutations in CANDLE/PRAAS patients promote type I IFN production. *J Clin Invest* 125, 4196–211 (2015). [PubMed: 26524591]
 31. Poli MC, Ebstein F, Nicholas SK, de Guzman MM, Forbes LR, Chinn IK, Mace EM, Vogel TP, Carisey AF, Benavides F, Coban-Akdemir ZH, Gibbs RA, Jhangiani SN, Muzny DM, Carvalho CMB, Schady DA, Jain M, Rosenfeld JA, Emrick L, Lewis RA, Lee B, Zieba BA, Küry S, Krüger E, Lupski JR, Bostwick BL, Orange JS. Heterozygous Truncating Variants in POMP Escape Nonsense-Mediated Decay and Cause a Unique Immune Dysregulatory Syndrome. *Am J Hum Genet* 102, 1126–1142 (2018). [PubMed: 29805043]
 32. de Jesus AA, Brehm A, VanTries R, Pillet P, Parentelli AS, Montealegre Sanchez GA, Deng Z, Paut IK, Goldbach-Mansky R, Krüger E. Novel Proteasome Assembly Chaperone mutations in PSMG2/PAC2, cause the autoinflammatory interferonopathy, CANDLE/PRAAS4. *J Allergy Clin Immunol* 143, 1939–1943 (2019). [PubMed: 30664889]
 33. Sarabay G, Méchin D, Salhi A, Boursier G, Rittore C, Crow Y, Rice G, Tran TA, Cezar R, Duffy D, Bondet V, Boudhane L, Broca C, Kant BP, VanGijn M, Grandemange S, Richard E, Apparailly F, Toutou I. PSMB10, the last immunoproteasome gene missing for PRAAS. *J Allergy Clin Immunol* 145, 1015–1017.e6 (2020). [PubMed: 31783057]
 34. Küry S, Besnard T, Ebstein F, Khan TN, Gambin T, Douglas J, Bacino CA, Sanders SJ, Lehmann A, Latypova X, Khan K, Pacault M, Sacharow S, Glaser K, Bieth E, Perrin-Sabourin L, Jacquemont M-L, Cho MT, Roeder E, Denommé-Pichon A-S, Monaghan KG, Yuan B, Xia F, Simon S, Bonneau D, Parent P, Gilbert-Dussardier B, Odent S, Toutain A, Pasquier L, Barbooth D, Shaw CA, Patel A, Smith JL, Bi W, Schmitt S, Deb W, Nizon M, Mercier S, Vincent M, Rooryck C, Malan V, Briceño I, Gómez A, Nugent KM, Gibson JB, Cogné B, Lupski JR, Stessman HAF, Eichler EE, Retterer K, Yang Y, Redon R, Katsanis N, Rosenfeld JA, Kloetzel P-M, Golzio C, Bézieau S, Stankiewicz P, Isidor B. De Novo Disruption of the Proteasome Regulatory Subunit PSMD12 Causes a Syndromic Neurodevelopmental Disorder. *Am J Hum Genet* 100, 352–363 (2017). [PubMed: 28132691]
 35. Isidor B, Ebstein F, Hurst A, Vincent M, Bader I, Rudy NL, Cogne B, Mayr J, Brehm A, Bupp C, Warren K, Bacino CA, Gerard A, Ranells JD, Metcalfe KA, van Bever Y, Jiang YH, Mendelssohn BA, Cope H, Rosenfeld JA, Blackburn PR, Goodenberger ML, Kearney HM, Kennedy J, Scurr I, Szczaluba K, Ploski R, de Saint Martin A, Alembik Y, Piton A, Bruel AL, Thauvin-Robinet C, Strong A, Diderich KEM, Bourgeois D, Dahan K, Vignard V, Bonneau D, Colin E, Barth M, Camby C, Baujat G, Briceño I, Gómez A, Deb W, Conrad S, Besnard T, Bézieau S, Krüger E, Küry S, Stankiewicz P. Stankiewicz-Isidor syndrome: expanding the clinical and molecular phenotype. *Genet Med* 24, 179–191 (2022). [PubMed: 34906456]
 36. Yan K, Zhang J, Lee PY, Tao P, Wang J, Wang S, Zhou Q, Dong M. Haploinsufficiency of PSMD12 Causes Proteasome Dysfunction and Subclinical Autoinflammation. *Arthritis Rheumatol* 74, 1083–1090 (2022). [PubMed: 35080150]
 37. d'Angelo DM, di Filippo P, Breda L, Chiarelli F, Type I Interferonopathies in Children: An Overview. *Front Pediatr* 9, 631329 (2021) [PubMed: 33869112]
 38. Savic S, Coe J, Laws P. Autoinflammation: Interferonopathies and Other Autoinflammatory Diseases. *J Invest Dermatol* 142, 781–792 (2022). [PubMed: 34887082]
 39. Crow YJ, Stetson DB. The type I interferonopathies: 10 years on. *Nat Rev Immunol* 22 (2022), doi:10.1038/s41577-021-00633-9.

40. Baux D, van Goethem C, Ardouin O, Guignard T, Bergougnoux A, Koenig M, Roux AF. MobiDetails: online DNA variants interpretation. *Eur J Hum Genet* 29, 356–360 (2021). [PubMed: 33161418]
41. Hsieh TC, Bar-Haim A, Moosa S, Ehmke N, Gripp KW, Pantel JT, Danyel M, Mensah MA, Horn D, Rosnev S, Fleischer N, Bonini G, Hustinx A, Schmid A, Knaus A, Javanmardi B, Klinkhammer H, Lesmann H, Sivalingam S, Kamphans T, Meiswinkel W, Ebstein F, Krüger E, Küry S, Bézieau S, Schmidt A, Peters S, Engels H, Mangold E, Kreiß M, Cremer K, Perne C, Betz RC, Bender T, Grundmann-Hauser K, Haack TB, Wagner M, Brunet T, Bentzen HB, Averdunk L, Coetzer KC, Lyon GJ, Spielmann M, Schaaf CP, Mundlos S, Nöthen MM, Krawitz PM. GestaltMatcher facilitates rare disease matching using facial phenotype descriptors. *Nat Genet* 54, 349–357 (2022). [PubMed: 35145301]
42. Tully T, Quinn WG. Classical conditioning and retention in normal and mutant *Drosophila melanogaster*. *J Comp Physiol A* 157, 263–77 (1985). [PubMed: 3939242]
43. Küry S, van Woerden GM, Besnard T, Proietti Onori M, Latypova X, Towne MC, Cho MT, Prescott TE, Ploeg MA, Sanders S, Stessman HAF, Pujol A, Distel B, Robak LA, Bernstein JA, Denommé-Pichon AS, Lesca G, Sellars EA, Berg J, Carré W, Busk ØL, van Bon BWM, Waugh JL, Deardorff M, Hoganson GE, Bosanko KB, Johnson DS, Dabir T, Holla ØL, Sarkar A, Tveten K, de Bellescize J, Braathen GJ, Terhal PA, Grange DK, van Haeringen A, Lam C, Mirzaa G, Burton J, Bhoj EJ, Douglas J, Santani AB, Nesbitt AI, Helbig KL, Andrews M. v., Begtrup A, Tang S, van Gassen KLI, Juusola J, Foss K, Enns GM, Moog U, Hinderhofer K, Paramasivam N, Lincoln S, Kusako BH, Lindenbaum P, Charpentier E, Nowak CB, Cherot E, Simonet T, Ruivenkamp CAL, Hahn S, Brownstein CA, Xia F, Schmitt S, Deb W, Bonneau D, Nizon M, Quinquis D, Chelly J, Rudolf G, Sanlaville D, Parent P, Gilbert-Dussardier B, Toutain A, Sutton VR, Thies J, Peart-Vissers LELM, Boisseau P, Vincent M, Grabrucker AM, Dubourg C, Tan WH, Verbeek NE, Granzow M, Santen GWE, Shendure J, Isidor B, Pasquier L, Redon R, Yang Y, State MW, Kleefstra T, Cogné B, Petrovski S, Retterer K, Eichler EE, Rosenfeld JA, Agrawal PB, Bézieau S, Odent S, Elgersma Y, Mercier S. De Novo Mutations in Protein Kinase Genes CAMK2A and CAMK2B Cause Intellectual Disability. *Am J Hum Genet* 101, 768–788 (2017). [PubMed: 29100089]
44. Schembri L, Dalibart R, Tomasello F, Legembre P, Ichas F, de Giorgi F. The HA tag is cleaved and loses immunoreactivity during apoptosis. *Nat Methods* 4, 107–8 (2007) [PubMed: 17264856]
45. Dong Y, Zhang S, Wu Z, Li X, Wang WL, Zhu Y, Stoilova-McPhie S, Lu Y, Finley D, Mao Y. Cryo-EM structures and dynamics of substrate-engaged human 26S proteasome. *Nature* 565, 49–55 (2019). [PubMed: 30479383]
46. Shmueli MD, Sheban D, Eisenberg-Lerner A, Merbl Y. Histone degradation by the proteasome regulates chromatin and cellular plasticity. *FEBS J* 289, 3304–3316 (2022). [PubMed: 33914417]
47. McConkey DJ. The integrated stress response and proteotoxicity in cancer therapy. *Biochem Biophys Res Commun* 482, 450–453 (2017). [PubMed: 28212730]
48. Marzec M, Eletto D, Argon Y. GRP94: An HSP90-like protein specialized for protein folding and quality control in the endoplasmic reticulum. *Biochim Biophys Acta Mol Cell Res* 1823, 774–87 (2012).
49. Radhakrishnan SK, Lee CS, Young P, Beskow A, Chan JY, Deshaies RJ. Transcription Factor Nrf1 Mediates the Proteasome Recovery Pathway after Proteasome Inhibition in Mammalian Cells. *Mol Cell* 38, 17–28 (2010). [PubMed: 20385086]
50. Steffen J, Seeger M, Koch A, Krüger E. Proteasomal degradation is transcriptionally controlled by TCF11 via an ERAD-dependent feedback loop. *Mol Cell* 40, 147–58 (2010). [PubMed: 20932482]
51. Kostyszyn B, Cowburn RF, Seiger Å, Kjældgaard A, Sundström E. Distribution of presenilin 1 and 2 and their relation to Notch receptors and ligands in human embryonic/foetal central nervous system. *Brain Res Dev Brain Res* 151, 75–86 (2004). [PubMed: 15246694]
52. Rice GI, Melki I, Frémond ML, Briggs TA, Rodero MP, Kitabayashi N, Oojageer A, Bader-Meunier B, Belot A, Bodemer C, Quartier P, Crow YJ. Assessment of Type I Interferon Signaling in Pediatric Inflammatory Disease. *J Clin Immunol* 37, 123–132 (2017). [PubMed: 27943079]
53. Ebstein F, Lange N, Urban S, Seifert U, Krüger E, Kloetzel PM. Maturation of human dendritic cells is accompanied by functional remodelling of the ubiquitin-proteasome system. *Int J Biochem Cell Biol* 41, 1205–1215 (2009). [PubMed: 19028597]

54. Tesser A, Piperno GM, Pin A, Piscianz E, Boz V, Benvenuti F, Tommasini A. Priming of the cGAS-STING-TBK1 pathway enhances LPS-induced release of type I interferons. *Cells* 10, 785 (2021). [PubMed: 33916318]
55. Bedford L, Hay D, Devoy A, Paine S, Powe DG, Seth R, Gray T, Topham I, Fone K, Rezvani N, Mee M, Soane T, Layfield R, Sheppard PW, Ebendal T, Usoskin D, Lowe J, Mayer RJ. Depletion of 26S proteasomes in mouse brain neurons causes neurodegeneration and lewy-like inclusions resembling human pale bodies. *J Neurosci* 28, 8189–98 (2008). [PubMed: 18701681]
56. Tashiro Y, Urushitani M, Inoue H, Koike M, Uchiyama Y, Komatsu M, Tanaka K, Yamazaki M, Abe M, Misawa H, Sakimura K, Ito H, Takahashia R. Motor neuron-specific disruption of proteasomes, but not autophagy, replicates amyotrophic lateral sclerosis. *J Biol Chem* 287, 42984–94 (2012). [PubMed: 23095749]
57. Kröll-Hermi A, Ebstein F, Stoetzel C, Geoffroy V, Schaefer E, Scheidecker S, Bär S, Takamiya M, Kawakami K, Zieba BA, Studer F, Pelletier V, Eyer mann C, Speeg-Schatz C, Laugel V, Lipsker D, Sandron F, McGinn S, Boland A, Deleuze J, Kuhn L, Chicher J, Hammann P, Friant S, Etard C, Krüger E, Muller J, Strähle U, Dollfus H. Proteasome subunit PSMC3 variants cause neurosensory syndrome combining deafness and cataract due to proteotoxic stress. *EMBO Mol Med* 12, e11861 (2020). [PubMed: 32500975]
58. Reed P, Watts H, Truzoli R. Flexibility in young people with autism spectrum disorders on a card sort task. *Autism* 17, 162–71 (2013). [PubMed: 21690212]
59. Leung RC, Zakzanis KK. Brief report: Cognitive flexibility in autism spectrum disorders: A quantitative review. *J Autism Dev Disord* 44, 2628–45 (2014). [PubMed: 24862496]
60. Tully T, Boyton S, Brandes C, Dura JM, Mihalek R, Preat T, Vilella A. Genetic dissection of memory formation in *Drosophila melanogaster*. *Cold Spring Harb Symp Quant Biol* 55, 203–11 (1990). [PubMed: 2132815]
61. Swanson R, Rogers RD, Sahakian BJ, Summers BA, Polkey CE, Robbins TW. Probabilistic learning and reversal deficits in patients with Parkinson's disease or frontal or temporal lobe lesions: Possible adverse effects of dopaminergic medication. *Neuropsychologia* 38, 596–612 (2000). [PubMed: 10689037]
62. Remijnse PL, Nielen MMA, van Balkom AJLM, Cath DC, van Oppen P, Uylings HBM, Veltman DJ. Reduced orbitofrontal-striatal activity on a reversal learning task in obsessive-compulsive disorder. *Arch Gen Psychiatry* 63, 1225–36 (2006). [PubMed: 17088503]
63. Finger EC, Marsh AA, Mitchell DG, Reid ME, Sims C, Budhani S, Kosson DS, Chen G, Towbin KE, Leibenluft E, Pine DS, Blair JR. Abnormal ventromedial prefrontal cortex function in children with psychopathic traits during reversal learning. *Arch Gen Psychiatry* 65, 586–94 (2008). [PubMed: 18458210]
64. Leeson VC, Robbins TW, Matheson E, Hutton SB, Ron MA, Barnes TRE, Joyce EM. Discrimination Learning, Reversal, and Set-Shifting in First-Episode Schizophrenia: Stability Over Six Years and Specific Associations with Medication Type and Disorganization Syndrome. *Biol Psychiatry* 66, 586–93 (2009). [PubMed: 19576575]
65. Izquierdo A, Jentsch JD. Reversal learning as a measure of impulsive and compulsive behavior in addictions. *Psychopharmacology (Berl)* 219, 607–20 (2012). [PubMed: 22134477]
66. Smolen P, Baxter DA, Byrne JH, Paradoxical LTP maintenance with inhibition of protein synthesis and the proteasome suggests a novel protein synthesis requirement for early LTP reversal. *J Theor Biol* 457, 79–87 (2018). [PubMed: 30138630]
67. Dong C, Bach S. v., Haynes KA, Hegde AN. Proteasome modulates positive and negative translational regulators in long-term synaptic plasticity. *J Neurosci* 34, 3171–82 (2014). [PubMed: 24573276]
68. Wilhelmsson U, Pozo-Rodríguez A, Kalm M, de Pablo Y, Widestrand Å, Pekna M, Pekny M. The role of GFAP and vimentin in learning and memory. *Biol Chem* 400, 1147–1156 (2019). [PubMed: 31063456]
69. Hausrat TJ, Muhia M, Gerrow K, Thomas P, Hirdes W, Tsukita S, Heisler FF, Herich L, Dubroqua S, Breiden P, Feldon J, Schwarz JR, Yee BK, Smart TG, Triller A, Kneussel M. Radixin regulates synaptic GABA A receptor density and is essential for reversal learning and short-term memory. *Nat Commun* 6, 6872 (2015). [PubMed: 25891999]

70. DePoy LM, Gourley SL. Synaptic Cytoskeletal Plasticity in the Prefrontal Cortex Following Psychostimulant Exposure. *Traffic* 16, 919–40 (2015). [PubMed: 25951902]
71. Wall MJ, Collins DR, Chery SL, Allen ZD, Pastuzyn ED, George AJ, Nikolova VD, Moy SS, Philpot BD, Shepherd JD, Müller J, Ehlers MD, Mabb AM, Corrêa SAL. The Temporal Dynamics of Arc Expression Regulate Cognitive Flexibility. *Neuron* 98, 1124–1132 (2018). [PubMed: 29861284]
72. Sung MK, Reitsma JM, Sweredoski MJ, Hess S, Deshaies RJ. Ribosomal proteins produced in excess are degraded by the ubiquitin-proteasome system. *Mol Biol Cell* 27, 2642–52 (2016). [PubMed: 27385339]
73. Hetman M, Slomnicki LP. Ribosomal biogenesis as an emerging target of neurodevelopmental pathologies. *J Neurochem* 148, 325–347 (2019). [PubMed: 30144322]
74. Bourque DK, Hartley T, Nikkel SM, Pohl D, Tétreault M, Kernohan KD, Dymont DA. A de novo mutation in RPL10 causes a rare X-linked ribosomopathy characterized by syndromic intellectual disability and epilepsy: A new case and review of the literature. *Eur J Med Genet* 61, 89–93 (2018). [PubMed: 29066376]
75. Crow YJ, Manel N. Aicardi-Goutières syndrome and the type I interferonopathies. *Nat Rev Immunol* 15, 429–40 (2015). [PubMed: 26052098]
76. Livingston JH, Crow YJ. Neurologic phenotypes associated with mutations in TREX1, RNASEH2A, RNASEH2B, RNASEH2C, SAMHD1, ADAR1, and IFIH1: Aicardi-Goutières syndrome and beyond. *Neuropediatrics* 47, 355–360 (2016). [PubMed: 27643693]
77. Araya P, Waugh KA, Sullivan KD, Núñez NG, Roselli E, Smith KP, Granrath RE, Rachubinski AL, Estrada BE, Butcher ET, Minter R, Tuttle KD, Bruno TC, Maccioni M, Espinosa JM. Trisomy 21 dysregulates T cell lineages toward an autoimmunity-prone state associated with interferon hyperactivity. *Proc Natl Acad Sci U S A* 116, 24231–24241 (2019). [PubMed: 31699819]
78. Waugh KA, Araya P, Pandey A, Jordan KR, Smith KP, Granrath RE, Khanal S, Butcher ET, Estrada BE, Rachubinski AL, McWilliams JA, Minter R, Dimasi T, Colvin KL, Baturin D, Pham AT, Galbraith MD, Bartsch KW, Yeager ME, Porter CC, Sullivan KD, Hsieh EW, Espinosa JM. Mass Cytometry Reveals Global Immune Remodeling with Multi-lineage Hypersensitivity to Type I Interferon in Down Syndrome. *Cell Rep* 29, 1893–1908 (2019). [PubMed: 31722205]
79. Sullivan KD, Lewis HC, Hill AA, Pandey A, Jackson LP, Cabral JM, Smith KP, Liggett LA, Gomez EB, Galbraith MD, Degregori J, Espinosa JM. Trisomy 21 consistently activates the interferon response. *Elife* 5, e16220 (2016). [PubMed: 27472900]
80. Sullivan KD, Evans D, Pandey A, Hraha TH, Smith KP, Markham N, Rachubinski AL, Wolter-Warmerdam K, Hickey F, Espinosa JM, Blumenthal T. Trisomy 21 causes changes in the circulating proteome indicative of chronic autoinflammation. *Sci Rep* 7, 14818 (2017). [PubMed: 29093484]
81. Akwa Y, Hassett DE, Eloranta M-L, Sandberg K, Masliah E, Powell H, Whitton JL, Bloom FE, Campbell IL. Transgenic Expression of IFN- α in the Central Nervous System of Mice Protects Against Lethal Neurotropic Viral Infection but Induces Inflammation and Neurodegeneration. *J Immunol* 161, 5016–26 (1998). [PubMed: 9794439]
82. Campbell IL, Krucker T, Steffensen S, Akwa Y, Powell HC, Lane T, Carr DJ, Gold LH, Henriksen SJ, Siggins GR. Structural and functional neuropathology in transgenic mice with CNS expression of IFN- α . *Brain Res* 835, 46–61 (1999). [PubMed: 10448195]
83. Kavanagh D, McGlasson S, Jury A, Williams J, Scolding N, Bellamy C, Gunther C, Ritchie D, Gale DP, Kanwar YS, Challis R, Buist H, Overell J, Weller B, Flossmann O, Blunden M, Meyer EP, Krucker T, Evans SJW, Campbell IL, Jackson AP, Chandran S, Hunt DPJ. Type I interferon causes thrombotic microangiopathy by a dose-dependent toxic effect on the microvasculature. *Blood* 128, 2824–2833 (2016). [PubMed: 27663672]
84. Goldmann T, Zeller N, Raasch J, Kierdorf K, Frenzel K, Ketscher L, Basters A, Staszewski O, Bredecke SM, Spiess A, Tay TL, Kreutz C, Timmer J, Mancini GM, Blank T, Fritz G, Biber K, Lang R, Malo D, Merkler D, Heikenwälder M, Knobloch K, Prinz M. USP 18 lack in microglia causes destructive interferonopathy of the mouse brain. *EMBO J* 34, 1612–29 (2015). [PubMed: 25896511]

85. Eggenberger J, Blanco-Melo D, Panis M, Brennand KJ, ten Oever BR. Type I interferon response impairs differentiation potential of pluripotent stem cells. *Proc Natl Acad Sci U S A* 116, 1384–1393 (2019). [PubMed: 30606801]
86. Yu Q, Katlinskaya Y. v., Carbone CJ, Zhao B, Katlinski K. v., Zheng H, Guha M, Li N, Chen Q, Yang T, Lengner CJ, Greenberg RA, Johnson FB, Fuchs SY. DNA-Damage-Induced Type I Interferon Promotes Senescence and Inhibits Stem Cell Function. *Cell Rep* 11, 785–797 (2015). [PubMed: 25921537]
87. Zhu K, Dunner K, McConkey DJ. Proteasome inhibitors activate autophagy as a cytoprotective response in human prostate cancer cells. *Oncogene* 29, 451–62 (2010). [PubMed: 19881538]
88. Studencka-Turski M, Çetin G, Junker H, Ebstein F, Krüger E. Molecular Insight Into the IRE1 α -Mediated Type I Interferon Response Induced by Proteasome Impairment in Myeloid Cells of the Brain. *Front Immunol* 10, 2900 (2019). [PubMed: 31921161]
89. Khacho M, Harris R, Slack RS. Mitochondria as central regulators of neural stem cell fate and cognitive function. *Nat Rev Neurosci* 20, 34–48 (2019). [PubMed: 30464208]
90. Yang K, Huang R, Fujihira H, Suzuki T, Yan N. N-glycanase NGLY1 regulates mitochondrial homeostasis and inflammation through NRF1. *J Exp Med* 215, 2600–2616 (2018). [PubMed: 30135079]
91. Sadler AJ, Williams BRG. Structure and function of the protein kinase R. *Curr Top Microbiol Immunol* 316, 253–92 (2007). [PubMed: 17969452]
92. Reid DW, Chen Q, Tay ASL, Shenolikar S, Nicchitta C. v.. The unfolded protein response triggers selective mRNA release from the endoplasmic reticulum. *Cell* 158, 1362–1374 (2014). [PubMed: 25215492]
93. Meurs E, Chong K, Galabru J, Thomas NSB, Kerr IM, Williams BRG, Hovanessian AG. Molecular cloning and characterization of the human double-stranded RNA-activated protein kinase induced by interferon. *Cell* 62, 379–90 (1990). [PubMed: 1695551]
94. Benkirane M, Neuveut C, Chun RF, Smith SM, Samuel CE, Gatignol A, Jeang KT. Oncogenic potential of TAR RNA binding protein TRBP and its regulatory interaction with RNA-dependent protein kinase PKR. *EMBO Journal* 16, 611–24 (1997). [PubMed: 9034343]
95. Patel RC, Sen GC. PACT, a protein activator of the interferon-induced protein kinase, PKR. *EMBO Journal* 17 (1998), doi:10.1093/emboj/17.15.4379.
96. Siwecka N, Rozp dek-Kami ska W, Wawrzynkiewicz A, Pytel D, Diehl JA, Majsterek I. The structure, activation and signaling of IRE1 and its role in determining cell fate. *Biomedicines* 9, 156 (2021). [PubMed: 33562589]
97. Deture MA, Dickson DW. The neuropathological diagnosis of Alzheimer’s disease. *Mol Neurodegener* 14, 32 (2019). [PubMed: 31375134]
98. Gal-Ben-Ari S, Barrera I, Ehrlich M, Rosenblum K. PKR: A kinase to remember. *Front Mol Neurosci* 11, 480 (2019). [PubMed: 30686999]
99. Marchal JA, Lopez GJ, Peran M, Comino A, Delgado JR, García-García JA, Conde V, Aranda FM, Rivas C, Esteban M, Garcia MA. The impact of PKR activation: From neurodegeneration to cancer. *FASEB J* 28, 1965–74 (2014). [PubMed: 24522206]
100. Chukwurah E, Farabaugh KT, Guan BJ, Ramakrishnan P, Hatzoglou M. A tale of two proteins: PACT and PKR and their roles in inflammation. *FEBS J* 288, 6365–6391 (2021). [PubMed: 33387379]
101. Muzio L, Viotti A, Martino G. Microglia in Neuroinflammation and Neurodegeneration: From Understanding to Therapy. *Front Neurosci* 15, 742065 (2021). [PubMed: 34630027]
102. Ahmed MM, Johnson NR, Boyd TD, Coughlan C, Chial HJ, Potter H. Innate Immune System Activation and Neuroinflammation in Down Syndrome and Neurodegeneration: Therapeutic Targets or Partners? *Front Aging Neurosci* 13, 718426 (2021). [PubMed: 34603007]
103. Sobreira N, Schiettecatte F, Valle D, Hamosh A. GeneMatcher: a matching tool for connecting investigators with an interest in the same gene. *Hum Mutat* 36, 928–930 (2015). [PubMed: 26220891]
104. Karczewski KJ, Francioli LC, Tiao G, Cummings BB, Alföldi J, Wang Q, Collins RL, Laricchia KM, Ganna A, Birnbaum DP, Gauthier LD, Brand H, Solomonson M, Watts NA, Rhodes D, Singer-Berk M, England EM, Seaby EG, Kosmicki JA, Walters RK, Tashman K, Farjoun Y,

Banks E, Poterba T, Wang A, Seed C, Whiffin N, Chong JX, Samocha KE, Pierce-Hoffman E, Zappala Z, O'Donnell-Luria AH, Minikel EV, Weisburd B, Lek M, Ware JS, Vittal C, Armean IM, Bergelson L, Cibulskis K, Connolly KM, Covarrubias M, Donnelly S, Ferriera S, Gabriel S, Gentry J, Gupta N, Jeandet T, Kaplan D, Llanwarne C, Munshi R, Novod S, Petrillo N, Roazen D, Ruano-Rubio V, Saltzman A, Schleicher M, Soto J, Tibbetts K, Tolonen C, Wade G, Talkowski ME, Aguilar Salinas CA, Ahmad T, Albert CM, Ardissino D, Atzmon G, Barnard J, Beaugerie L, Benjamin EJ, Boehnke M, Bonnycastle LL, Bottinger EP, Bowden DW, Bown MJ, Chambers JC, Chan JC, Chasman D, Cho J, Chung MK, Cohen B, Correa A, Dabelea D, Daly MJ, Darbar D, Duggirala R, Dupuis J, Ellinor PT, Elosua R, Erdmann J, Esko T, Färkkilä M, Florez J, Franke A, Getz G, Glaser B, Glatt SJ, Goldstein D, Gonzalez C, Groop L, Haiman C, Hanis C, Harms M, Hiltunen M, Holi MM, Hultman CM, Kallela M, Kaprio J, Kathiresan S, Kim BJ, Kim YJ, Kirov G, Kooner J, Koskinen S, Krumholz HM, Kugathasan S, Kwak SH, Laakso M, Lehtimäki T, Loos RJJ, Lubitz SA, Ma RCW, MacArthur DG, Marrugat J, Mattila KM, McCarroll S, McCarthy MI, McGovern D, McPherson R, Meigs JB, Melander O, Metspalu A, Neale BM, Nilsson PM, O'Donovan MC, Ongur D, Orozco L, Owen MJ, Palmer CNA, Palotie A, Park KS, Pato C, Pulver AE, Rahman N, Remes AM, Rioux JD, Ripatti S, Roden DM, Saleheen D, Salomaa V, Samani NJ, Scharf J, Schunkert H, Shoemaker MB, Sklar P, Soininen H, Sokol H, Spector T, Sullivan PF, Suvisaari J, Tai ES, Teo YY, Tiinamaija T, Tsuang M, Turner D, Tusie-Luna T, Vartiainen E, Watkins H, Weersma RK, Wessman M, Wilson JG, Xavier RJ, Neale BM, Daly MJ. The mutational constraint spectrum quantified from variation in 141,456 humans. *Nature* 581, 434–443 (2020). [PubMed: 32461654]

105. Taliun D, Harris DN, Kessler MD, Carlson J, Szpiech ZA, Torres R, Taliun SAG, Corvelo A, Gogarten SM, Kang HM, Pitsillides AN, LeFaive J, been Lee S, Tian X, Browning BL, Das S, Emde AK, Clarke WE, Loesch DP, Shetty AC, Blackwell TW, Smith A. v., Wong Q, Liu X, Conomos MP, Bobo DM, Aguet F, Albert C, Alonso A, Ardlie KG, Arking DE, Aslibekyan S, Auer PL, Barnard J, Barr RG, Barwick L, Becker LC, Beer RL, Benjamin EJ, Bielak LF, Blangero J, Boehnke M, Bowden DW, Brody JA, Burchard EG, Cade BE, Casella JF, Chalazan B, Chasman DI, Chen YDI, Cho MH, Choi SH, Chung MK, Clish CB, Correa A, Curran JE, Custer B, Darbar D, Daya M, de Andrade M, DeMeo DL, Dutcher SK, Ellinor PT, Emery LS, Eng C, Fatkin D, Fingerlin T, Forer L, Fornage M, Franceschini N, Fuchsberger C, Fullerton SM, Germer S, Gladwin MT, Gottlieb DJ, Guo X, Hall ME, He J, Heard-Costa NL, Heckbert SR, Irvin MR, Johnsen JM, Johnson AD, Kaplan R, Kardina SLR, Kelly T, Kelly S, Kenny EE, Kiel DP, Klemmer R, Konkle BA, Kooperberg C, Köttgen A, Lange LA, Lasky-Su J, Levy D, Lin X, Lin KH, Liu C, Loos RJJ, Garman L, Gerszten R, Lubitz SA, Lunetta KL, Mak ACY, Manichaikul A, Manning AK, Mathias RA, McManus DD, McGarvey ST, Meigs JB, Meyers DA, Mikulla JL, Minear MA, Mitchell BD, Mohanty S, Montasser ME, Montgomery C, Morrison AC, Murabito JM, Natale A, Natarajan P, Nelson SC, North KE, O'Connell JR, Palmer ND, Pankratz N, Peloso GM, Peyser PA, Pleinness J, Post WS, Psaty BM, Rao DC, Redline S, Reiner AP, Roden D, Rotter JI, Ruczinski I, Sarnowski C, Schoenherr S, Schwartz DA, Seo JS, Seshadri S, Sheehan VA, Sheu WH, Shoemaker MB, Smith NL, Smith JA, Sotoodehnia N, Stilp AM, Tang W, Taylor KD, Telen M, Thornton TA, Tracy RP, van den Berg DJ, Vasan RS, Viaud-Martinez KA, Vrieze S, Weeks DE, Weir BS, Weiss ST, Weng LC, Willer CJ, Zhang Y, Zhao X, Arnett DK, Ashley-Koch AE, Barnes KC, Boerwinkle E, Gabriel S, Gibbs R, Rice KM, Rich SS, Silverman EK, Qasba P, Gan W, Abe N, Almasy L, Ament S, Anderson P, Anugu P, Applebaum-Bowden D, Assimes T, Avramopoulos D, Barron-Casella E, Beaty T, Beck G, Becker D, Beitelshes A, Benos T, Bezerra M, Bis J, Bowler R, Broeckel U, Broome J, Bunting K, Bustamante C, Buth E, Cardwell J, Carey V, Carty C, Casaburi R, Castaldi P, Chaffin M, Chang C, Chang YC, Chavan S, Chen BJ, Chen WM, Chuang LM, Chung RH, Comhair S, Cornell E, Crandall C, Crapo J, Curtiss J, Damcott C, David S, Davis C, de las Fuentes L, DeBaun M, Deka R, Devine S, Duan Q, Duggirala R, Durda JP, Eaton C, Ekanwe L, el Boueiz A, Erzurum S, Farber C, Flickinger M, Fornage M, Frazer C, Fu M, Fulton L, Gao S, Gao Y, Gass M, Gelb B, Geng XP, Geraci M, Ghosh A, Gignoux C, Glahn D, Gong DW, Goring H, Graw S, Grine D, Gu CC, Guan Y, Gupta N, Haessler J, Hawley NL, Heavner B, Herrington D, Hersh C, Hidalgo B, Hixson J, Hobbs B, Hokanson J, Hong E, Hoth K, Hsiung CA, Hung YJ, Huston H, Hwu CM, Jackson R, Jain D, Jhun MA, Johnson C, Johnston R, Jones K, Kathiresan S, Khan A, Kim W, Kinney G, Kramer H, Lange C, Lange E, Lange L, Laurie C, LeBoff M, Lee J, Lee SS, Lee WJ, Levine D, Lewis J, Li X, Li Y, Lin H, Lin H, Lin KH, Liu S, Liu

Y, Liu Y, Luo J, Mahaney M, Make B, Manson JA, Margolin L, Martin L, Mathai S, May S, McArdle P, McDonald ML, McFarland S, McGoldrick D, McHugh C, Mei H, Mestroni L, Min N, Minster RL, Moll M, Moscati A, Musani S, Mwasongwe S, Mychaleckyj JC, Nadkarni G, Naik R, Naseri T, Nekhai S, Neltner B, Ochs-Balcom H, Paik D, Pankow J, Parsa A, Peralta JM, Perez M, Perry J, Peters U, Phillips LS, Pollin T, Becker JP, Boorgula MP, Preuss M, Qiao D, Qin Z, Rafaels N, Raffield L, Rasmussen-Torvik L, Ratan A, Reed R, Regan E, Reupena MS, Roselli C, Russell P, Ruuska S, Ryan K, Sabino EC, Saleheen D, Salimi S, Salzberg S, Sandow K, Sankaran VG, Scheller C, Schmidt E, Schwander K, Sciruba F, Seidman C, Seidman J, Sherman SL, Shetty A, Sheu WHH, Silver B, Smith J, Smith T, Smoller S, Snively B, Snyder M, Sofer T, Storm G, Streeten E, Sung YJ, Sylvia J, Szpiro A, Sztalryd C, Tang H, Taub M, Taylor M, Taylor S, Threlkeld M, Tinker L, Tirschwell D, Tishkoff S, Tiwari H, Tong C, Tsai M, Vaidya D, VandeHaar P, Walker T, Wallace R, Walts A, Wang FF, Wang H, Watson K, Wessel J, Williams K, Williams LK, Wilson C, Wu J, Xu H, Yanek L, Yang I, Yang R, Zaghoul N, Zekavat M, Zhao SX, Zhao W, Zhi D, Zhou X, Zhu X, Papanicolaou GJ, Nickerson DA, Browning SR, Zody MC, Zöllner S, Wilson JG, Cupples LA, Laurie CC, Jaquish CE, Hernandez RD, O'Connor TD, Abecasis GR. Sequencing of 53,831 diverse genomes from the NHLBI TOPMed Program. *Nature* 590, 290–299 (2021). [PubMed: 33568819]

106. Fonteneau JF, Larsson M, Somersan S, Sanders C, Münz C, Kwok WW, Bhardwaj N, Jotereau F. Generation of high quantities of viral and tumor-specific human CD4+ and CD8+ T-cell clones using peptide pulsed mature dendritic cells. *J Immunol Methods* 258, 111–126 (2001). [PubMed: 11684128]
107. Bolduc FV, Bell K, Cox H, Broadie KS, Tully T. Excess protein synthesis in *Drosophila* Fragile X mutants impairs long-term memory. *Nat Neurosci* 11, 1143–5 (2008). [PubMed: 18776892]
108. Tully T, Quinn WG. Classical conditioning and retention in normal and mutant *Drosophila melanogaster*. *J Comp Physiol A* 157, 263–77 (1985). [PubMed: 3939242]
109. Tully T, Boyton S, Brandes C, Dura JM, Mihalek R, Preat T, Vilella A. Genetic dissection of memory formation in *Drosophila melanogaster*. *Cold Spring Harb Symp on Quant Biol* 55, 203–11 (1990).
110. Palma Medina LM, Becker AK, Michalik S, Yedavally H, Raineri EJM, Hildebrandt P, Salazar MG, Surmann K, Pfortner H, Mekonnen SA, Salvati A, Kaderali L, Van Dijl JM, Völker U. Metabolic Cross-talk between Human Bronchial Epithelial Cells and Internalized *Staphylococcus aureus* as a Driver for Infection. *Mol Cell Proteomics* 18, 892–908 (2019). [PubMed: 30808728]
111. Suomi T, Elo LL. Enhanced differential expression statistics for data-independent acquisition proteomics. *Sci Rep* 7, 5869 (2017). [PubMed: 28724900]
112. Phipson B, Lee S, Majewski IJ, Alexander WS, Smyth GK. ROBUST HYPERPARAMETER ESTIMATION PROTECTS AGAINST HYPERVARIABLE GENES AND IMPROVES POWER TO DETECT DIFFERENTIAL EXPRESSION. *Ann Appl Stat* 10, 946–963 (2016). [PubMed: 28367255]
113. Perez-Riverol Y, Bai J, Bandla C, García-Seisdedos D, Hewapathirana S, Kamatchinathan S, Kundu DJ, Prakash A, Frericks-Zipper A, Eisenacher M, Walzer M, Wang S, Brazma A, Vizcaíno JA. The PRIDE database resources in 2022: A hub for mass spectrometry-based proteomics evidences. *Nucleic Acids Res* 50, D543–D552 (2022). [PubMed: 34723319]
114. Hsieh TC, Bar-Haim A, Moosa S, Ehmke N, Gripp KW, Pantel JT, Danyel M, Mensah MA, Horn D, Rosnev S, Fleischer N, Bonini G, Hustinx A, Schmid A, Knaus A, Javanmardi B, Klinkhammer H, Lesmann H, Sivalingam S, Kamphans T, Meiswinkel W, Ebstein F, Krüger E, Küry S, Bézieau S, Schmidt A, Peters S, Engels H, Mangold E, Kreiß M, Cremer K, Perne C, Betz RC, Bender T, Grundmann-Hauser K, Haack TB, Wagner M, Brunet T, Bentzen HB, Averdunk L, Coetzer KC, Lyon GJ, Spielmann M, Schaaf CP, Mundlos S, Nöthen MM, Krawitz PM. GestaltMatcher facilitates rare disease matching using facial phenotype descriptors. *Nat Genet* 54, 349–357 (2022). [PubMed: 35145301]
115. Knaus A, Pantel JT, Pendziwiat M, Hajjir N, Zhao M, Hsieh TC, Schubach M, Gurovich Y, Fleischer N, Jäger M, Köhler S, Muhle H, Korff C, Möller RS, Bayat A, Calvas P, Chassaing N, Warren H, Skinner S, Louie R, Evers C, Bohn M, Christen HJ, van den Born M, Obersztyn E, Charzewska A, Endziniene M, Kortüm F, Brown N, Robinson PN, Schelhaas HJ, Weber Y, Helbig I, Mundlos S, Horn D, Krawitz PM. Characterization of glycosylphosphatidylinositol

- biosynthesis defects by clinical features, flow cytometry, and automated image analysis. *Genome Med* 10, 3 (2018). [PubMed: 29310717]
116. Marbach F, Rustad CF, Riess A, Ueki D, Hsieh TC, Jobani I, Prescott T, Bevo A, Erger F, Houge G, Redfors M, Altmueller J, Stokowy T, Gilissen C, Kubisch C, Scarano E, Mazzanti L, Fiskerstrand T, Krawitz PM, Lessel D, Netzer C. The Discovery of a LEMD2-Associated Nuclear Envelopathy with Early Progeroid Appearance Suggests Advanced Applications for AI-Driven Facial Phenotyping. *Am J Hum Genet* 104, 749 (2019). [PubMed: 30905398]
117. Oti M, Huynen MA, Brunner HG. Phenome connections. *Trends Genet* 24, 103–106 (2008). [PubMed: 18243400]
118. Gurovich Y, Hanani Y, Bar O, Nadav G, Fleischer N, Gelbman D, Basel-Salmon L, Krawitz PM, Kamphausen SB, Zenker M, Bird LM, Gripp KW. Identifying facial phenotypes of genetic disorders using deep learning. *Nat Med* 25, 60–64 (2019). [PubMed: 30617323]
119. Küry S, van Woerden GM, Besnard T, Proietti Onori M, Latypova X, Towne MC, Cho MT, Prescott TE, Ploeg MA, Sanders S, Stessman HAF, Pujol A, Distel B, Robak LA, Bernstein JA, Denommé-Pichon AS, Lesca G, Sellars EA, Berg J, Carré W, Busk ØL, van Bon BW, Waugh JL, Deardorff M, Hoganson GE, Bosanko KB, Johnson DS, Dabir T, Holla ØL, Sarkar A, Tveten K, de Bellescize J, Braathen GJ, Terhal PA, Grange DK, van Haeringen A, Lam C, Mirzaa G, Burton J, Bhoj EJ, Douglas J, Santani AB, Nesbitt AI, Helbig KL, Andrews MV, Begtrup A, Tang S, van Gassen KLI, Juusola J, Foss K, Enns GM, Moog U, Hinderhofer K, Paramasivam N, Lincoln S, Kusako BH, Lindenbaum P, Charpentier E, Nowak CB, Cherot E, Simonet T, Ruivenkamp CAL, Hahn S, Brownstein CA, Xia F, Schmitt S, Deb W, Bonneau D, Nizon M, Quinquis D, Chelly J, Rudolf G, Sanlaville D, Parent P, Gilbert-Dussardier B, Toutain A, Sutton VR, Thies J, Peart-Vissers LELM, Boisseau P, Vincent M, Grabrucker AM, Dubourg C, Tan WH, Verbeek NE, Granzow M, Santen GWE, Shendure J, Isidor B, Pasquier L, Redon R, Yang Y, State MW, Kleefstra T, Cogné B, Petrovski S, Retterer K, Eichler EE, Rosenfeld JA, Agrawal PB, Bézieau S, Odent S, Elgersma Y, Mercier S, De Novo Mutations in Protein Kinase Genes CAMK2A and CAMK2B Cause Intellectual Disability. *Am J Hum Genet* 101, 768–788 (2017). [PubMed: 29100089]
120. Goslin K, Banker G. Rapid changes in the distribution of GAP-43 correlate with the expression of neuronal polarity during normal development and under experimental conditions. *J Cell Biol* 110, 1319–31 (1990). [PubMed: 2139034]

OVERLINE: NEURODEVELOPMENTAL DISORDERS

One Sentence Summary:

PSMC3 variants associated with neurodevelopmental disorders lead to a type I interferon response by T cells that can be blocked by protein kinase R inhibition.

Editor's summary:

Insights into pathogenic proteasome variants

Pathogenic proteasome gene variants are associated with a broad spectrum of diseases. Ebstein and colleagues identified fifteen de novo missense variants in the *PSMC3* proteasome gene in patients with neurodevelopmental delay. Expression of *PSMC3* variants in mouse neuronal cultures led to altered dendrite development, and deletion of the fly *PSMC3* ortholog resulted in learning deficits in the fruit flies. Proteasome dysfunction in T cells from patients with *PSMC3* variants led to upregulation of proteotoxic markers and production of interferon type 1 that could be alleviated by inhibition of protein kinase R. These findings implicate *PSMC3* pathogenic variants in neurodevelopmental disorders and suggest a therapeutic strategy for patients carrying these missense mutations. ---DN

Author Manuscript

Author Manuscript

Author Manuscript

Author Manuscript

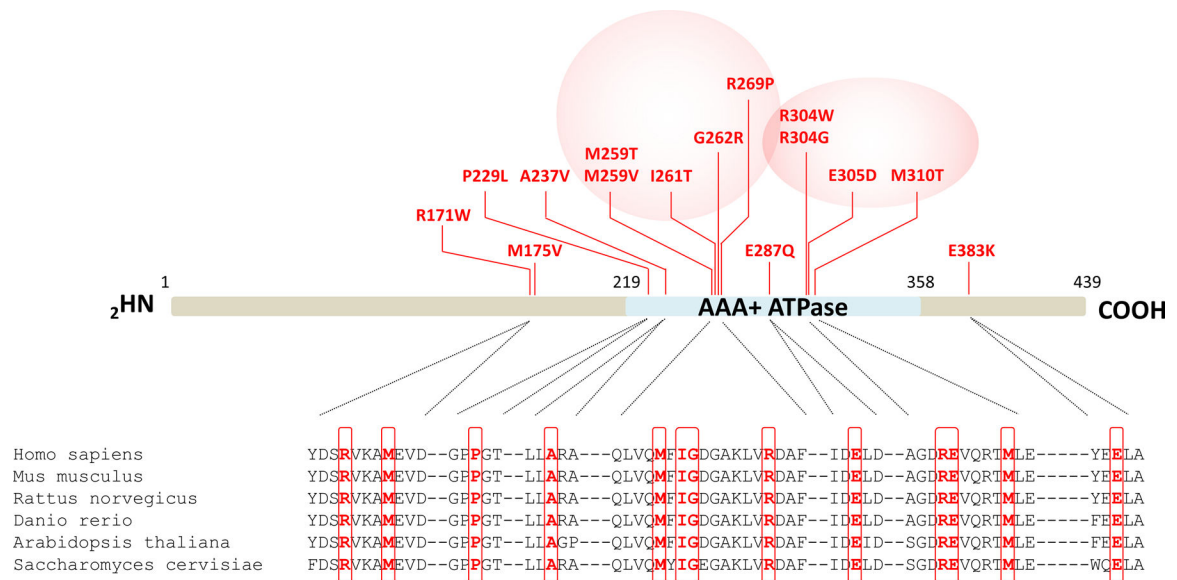


Fig. 1: Distribution of the *de novo* heterozygous PSMC3/Rpt5 variants identified in patients. Shown are the locations of the fifteen NDD-causing missense variants (indicated in red) along the PSMC3/Rpt5 protein. The AAA-ATPase domain of the PSMC3/Rpt5 proteasome subunit of the 19S regulatory particle is depicted in blue. Pink circles indicate the presence of variants hotspots. Shown is also a sequence alignment of regions immediately adjacent to the amino acids subjected to missense substitutions. Comparison of the PSMC3/Rpt5 primary structure across six eukaryotic organisms indicates the high conservation of the missense variant residues identified in NDD/ID patients which are highlighted by red boxes.

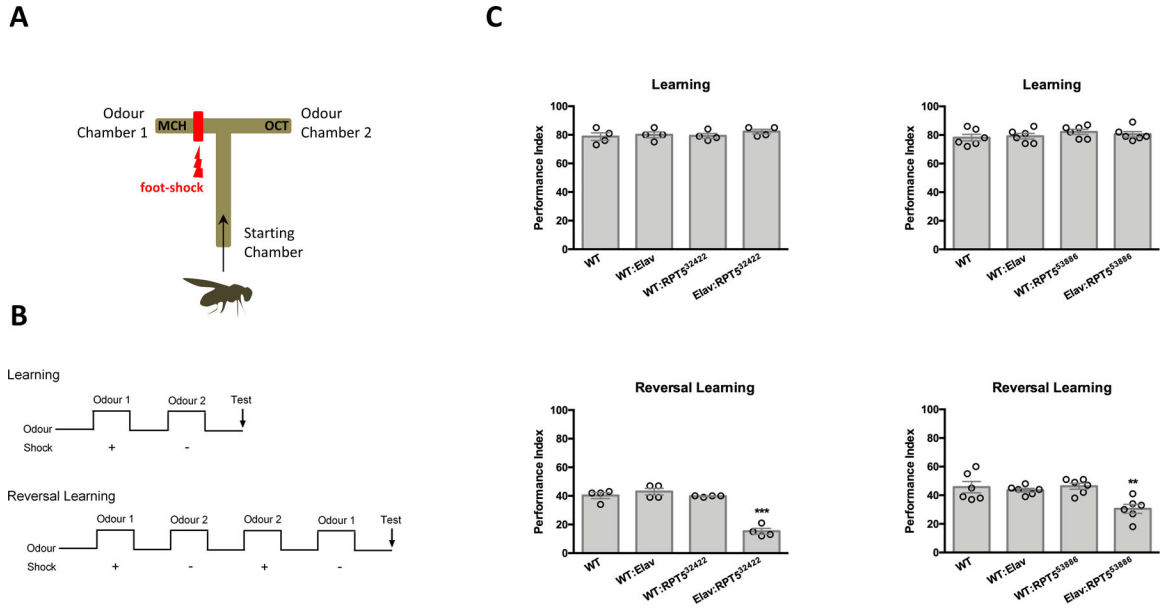


Fig. 2: Pan-neuronal RNAi-mediated knockdown of PSMC3/Rpt5 results in normal learning performance but defective reversal learning performance.

A. Shown is an illustration of a T-maze used for conditioning of odor-avoidance in *Drosophila*. Flies were trained to avoid one particular odor chamber that was associated with a foot-shock (in this example, odor chamber 1). **B.** The time course of the learning and reversal learning protocols used in these experiments is illustrated. Reversal learning was assessed by reversing odor shock pairing (4-methylcyclohexanol, MCH⁻; 3-octanol, OCT⁺), as indicated. **C.** Upper left: Shown is the learning performance index of wildtype flies (WT), flies expressing elav, flies with full expression of Rpt5³²⁴²² RNAi (WT: Rpt5³²⁴²²) and flies with pan-neuronal expression of Rpt5³²⁴²² RNAi (Elav: Rpt5³²⁴²²) (P=0.6435, N=4). Upper right: Shown is the learning performance index of wildtype flies (WT), flies expressing elav (WT:Elav), flies with full expression of Rpt5⁵³⁸⁸⁶ RNAi (WT: Rpt5⁵³⁸⁸⁶) and flies with pan-neuronal expression of Rpt5⁵³⁸⁸⁶ RNAi (Elav: Rpt5⁵³⁸⁸⁶) (P=0.5282, N=6; Upper right). Lower left: Shown is the reversal learning performance of all group described in C, Upper left. (P<0.0001, N=4). Lower right: Shown is the reversal learning performance index for all groups described in C, Upper right (P=0.0022, N=6). Statistical analysis was performed using ANOVA and then Tukey tests in JMP (SAS).**, P<0.01; ***, P<0.001.

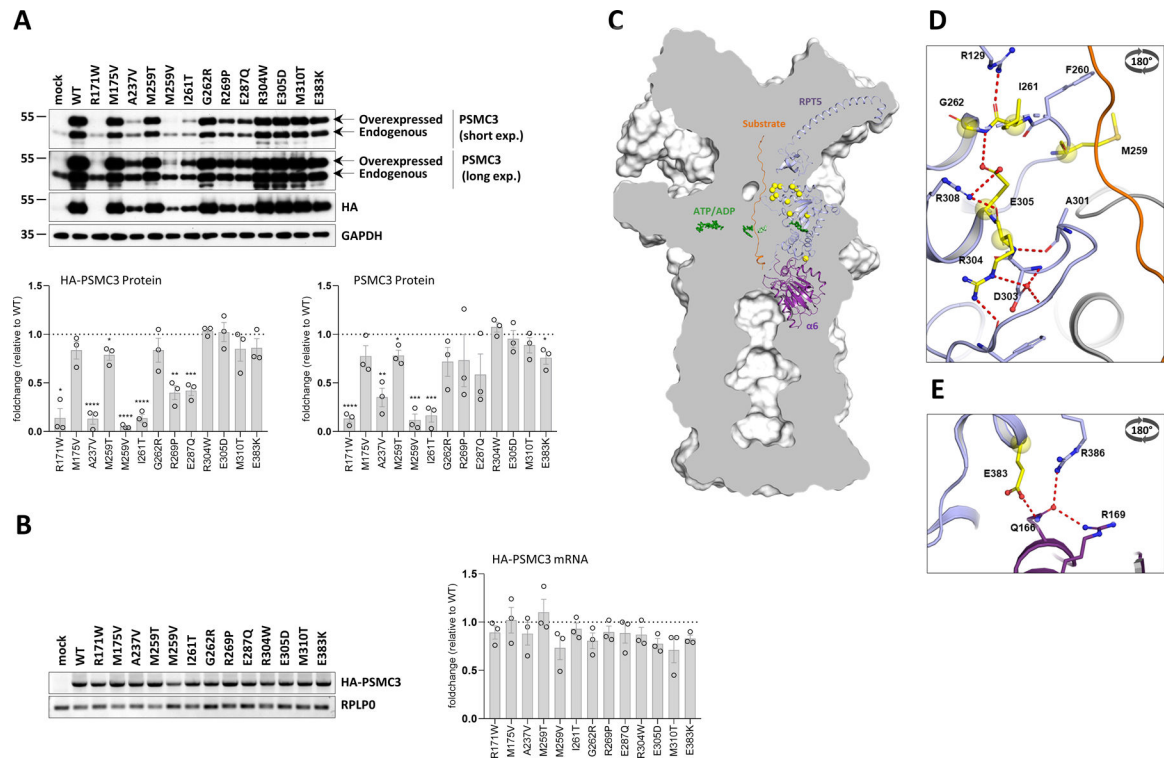


Fig. 3: PSMC3/Rpt5 protein variants do not behave similarly at the molecular level.

A. Top: SHSY5Y cells were transfected with HA-tagged *PSMC3* mutants for 24 h before protein extraction and Western-blotting using antibodies specific for PSMC3/Rpt5 and HA, as indicated. Non-transfected and mock-transfected cells served as negative controls. Equal protein loading was ensured by probing the membranes with an anti- α -tubulin monoclonal antibody (two exposure times are shown). Arrows indicate overexpressed and endogenous PSMC3/Rpt5. Shown is one representative experiment out of three. Bottom: quantification of HA-tagged and untagged PSMC3/Rpt5 proteins in transfected SHSY5Y cells by densitometry. Data are presented as protein foldchanges to wild-type (WT) PSMC3/Rpt5 proteins whose densitometry measurements were set to 1 (gridline) after normalization with GAPDH. Shown are mean values \pm SEM from three independent experiments. Statistical significance was assessed by unpaired Student's test (* $p < 0.05$, ** $p < 0.01$, *** $p < 0.001$ and **** $p < 0.0001$). **B.** Left: SHSY5Y cells that were transfected with HA-*PSMC3* variants were subjected to total RNA extraction followed by semi-quantitative RT-PCR using primer located in *PSMC3* and the polyadenylation signal of the pcDNA3.1/*myc*-HIS expression vector (BGH). Equal loading between the samples was ensured by amplifying the *RPL0* gene, as indicated. Right: quantification of HA-tagged *PSMC3* transcripts in transfected SHSY5Y cells by densitometry. Data are presented as mRNA foldchanges to wild-type (WT) HA-*PSMC3* mRNA whose densitometry measurements were set to 1 (gridline) after normalization with *RPLP0*. Shown are mean values \pm SEM from three independent experiments. **C.** A sliced surface view of the 26S proteasome (grey) was superimposed with a cartoon representation of the subunit PSMC3/RPT5 (blue) and PSMB1/α6 (purple) as well as the substrate (orange). The ATP/ADP molecules of the AAA-ATPase ring are shown as green sticks, while the positions of the investigated missense variants are indicated as bright

yellow spheres. **D.** Detailed representation of the missense variants in the loop region of the N-terminal α/β domain. The residues affected by these variants are involved in a polar interaction network close to the substrate tunnel (view rotated by 180° around the x-axis). **E.** Close up view on the RPT5- $\alpha 6$ interface affected by the E383L variant. Residues affected by this variant are shown as bright yellow balls and sticks with atoms coloured by polarity (oxygen in red, nitrogen in blue and sulphur in dark yellow, view rotated by 180° around the x-axis).

proteasome complexes by densitometry, as indicated. Data are presented as activity (LLVY-AMC) and protein (α 6, PA28 α and PSMC3) foldchanges in Patients #13, #18 and #21 vs their father and/or mother whose densitometric measurements were set to 1 (gridline), as indicated. Columns indicate the foldchange mean values \pm SEM calculated from the five normalizations. Statistical significance was assessed by unpaired Student's test ($*p<0.05$).

Author Manuscript

Author Manuscript

Author Manuscript

Author Manuscript

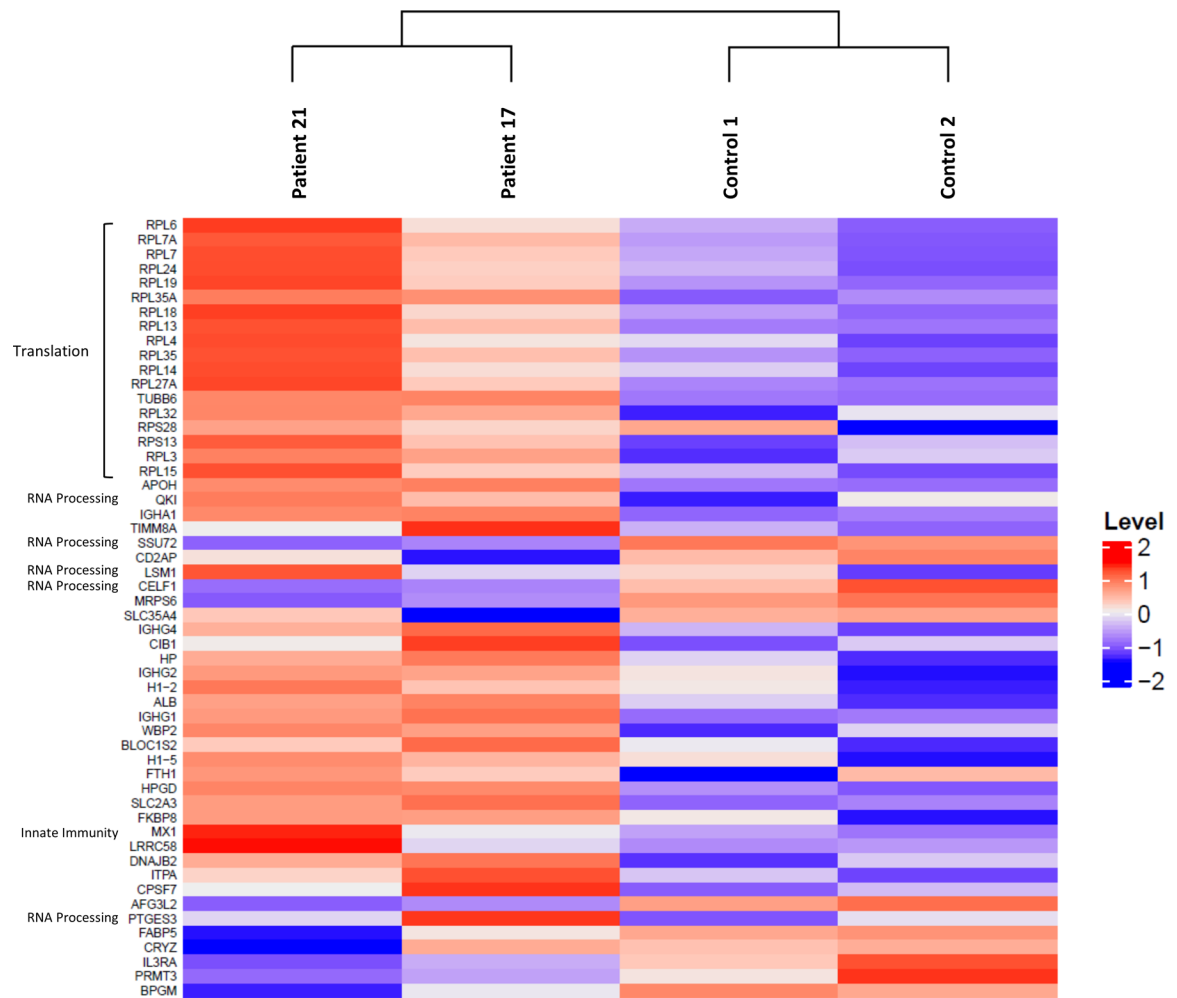


Fig. 5: Proteomic signatures of patients carrying *PSMC3/Rpt5* variants.

Heatmap cluster analysis showing the similarities in the protein expression profiles of the Patients #17 and #21 (carrying the R304W and E305D *PSMC3* variants, respectively) compared to their related controls (father and/or mother of the proband), as indicated. The heatmap indicates the normalized and scale expression value of proteins in the individual samples. Only the differentially expressed proteins with an absolute value of \log_2 fold-change greater than 2 were selected for the clustering analysis.

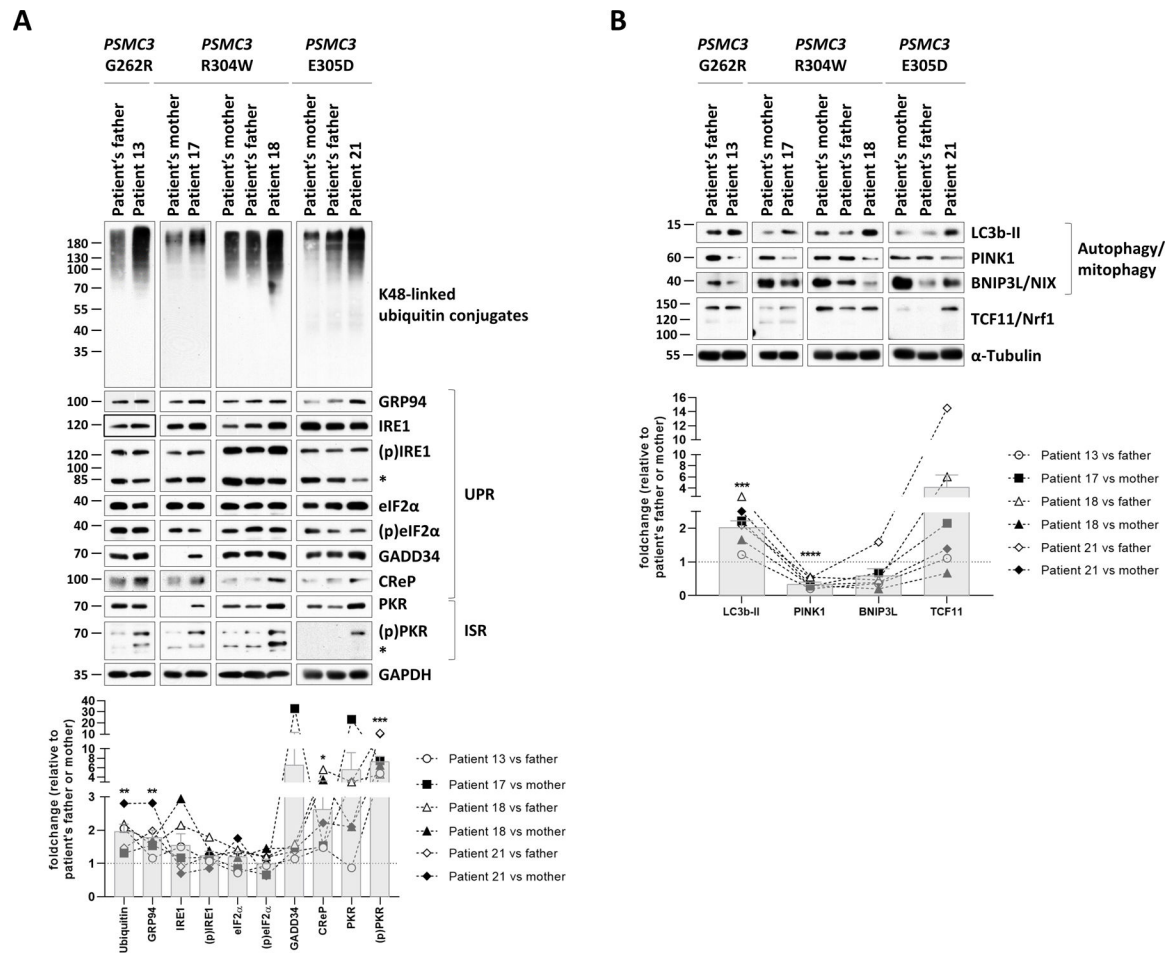


Fig. 6: T cells from patients carrying *PSMC3/Rpt5* variants exhibit signs of protein homeostasis perturbations and alterations of the UPR, ISR and autophagy/mitophagy pathways.

A. Top: five to twenty micrograms of RIPA lysates from T cells isolated from Patients #13, #17, #18 and #21 as well as related controls (*PSMC3* index case's father and/or mother) were separated by SDS-PAGE followed by Western-blotting using antibodies directed against K48-linked ubiquitin-modified proteins, GRP94, IRE1, phospho-IRE1, eIF2 α , phospho-eIF2 α , GADD34, CREP, PKR, phospho-PKR and GAPDH (loading control), as indicated. Bottom: Shown is the quantification of the Western-blot by densitometry. Data are presented as foldchanges in Patients #13, #17, #18 and #21 vs their father and/or mother whose densitometric measurements were set to 1 (gridline), as indicated. Columns indicate the foldchange mean values \pm SEM calculated from the six normalizations. Statistical significance was assessed by unpaired Student's test (* $p < 0.05$, ** $p < 0.01$ and *** $p < 0.001$).

B. Top: RIPA-cell lysates from Patients #13, #17, #18 and #21 as well as their related controls (index case's father and/or mother) were subjected to SDS-PAGE/Western-blotting using antibodies specific for LC3b, PINK1, BNIP3L and α -tubulin (loading control), as indicated. Bottom: quantification of the Western-blot by densitometry. Data are presented as protein foldchanges in Patients #13, #17, #18 and #21 vs their father and/or mother whose densitometric measurements were set to 1 (gridline), as indicated. Columns indicate

the foldchange mean values \pm SEM of the six normalizations. Statistical significance was assessed by unpaired Student's test (** $p < 0.001$ and **** $p < 0.0001$).

Author Manuscript

Author Manuscript

Author Manuscript

Author Manuscript

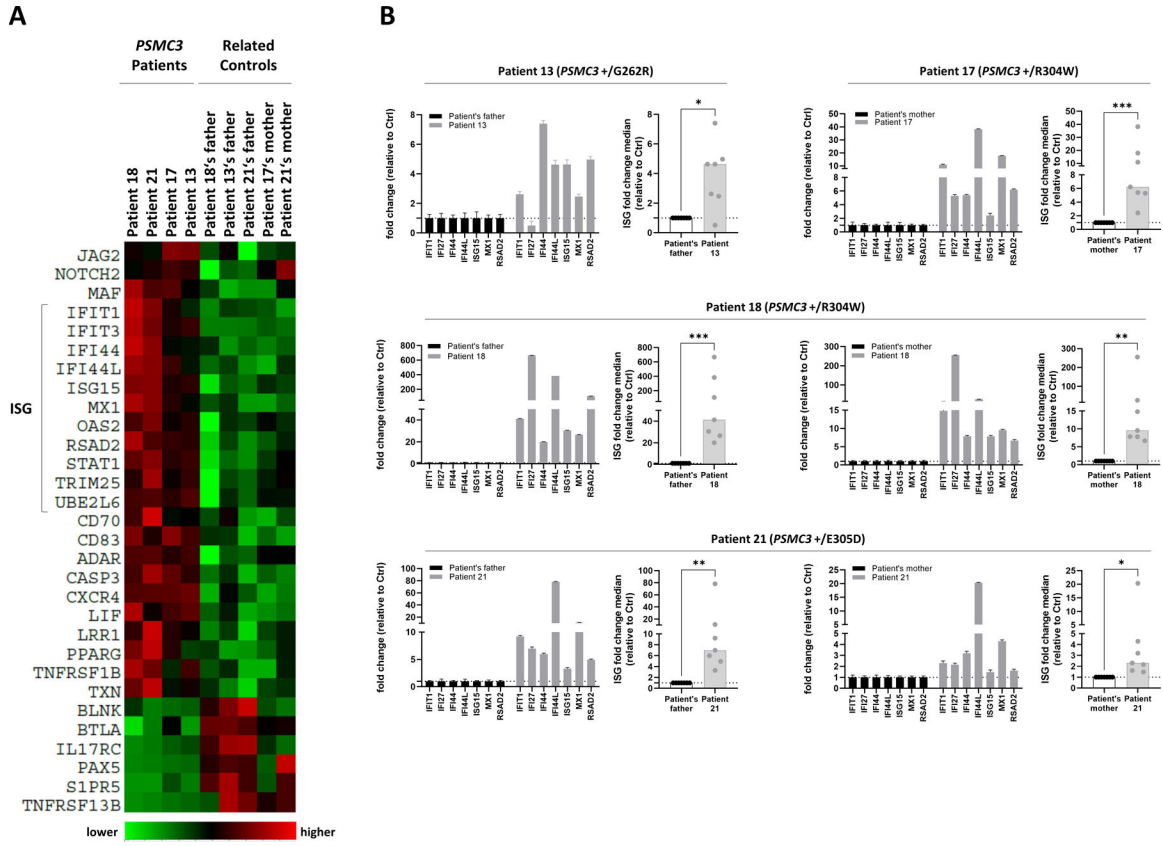


Fig. 7: T cells from patients with *PSMC3/Rpt5* missense variants exhibit a typical type I interferon (IFN) signature.

A. Heat map clustering of gene expression in T cells isolated from patients carrying a *PSMC3* variant and their relative controls (father and/or mother). Each column represents one individual patient or related control and each row represents one gene. Clustering of genes and samples was carried out by centred Pearson correlation. Colour indicates normalized counts of each transcript, with green representing higher expression and red relatively lower expression. **B.** Gene expression of seven typical IFN-stimulated genes (*IFIT1*, *IFI27*, *IFI44*, *IFI44L*, *ISG15*, *MX1* and *RSAD2*) was assayed by RT-qPCR on T cells derived from Patients #13, #17, #18 and #21 as well as their respective controls (the index case's father and/or mother). Expression levels were normalized to *GAPDH* and relative quantifications (RQ) are presented as fold change over controls. Shown is also the median fold expression of the seven ISGs over relative controls. Statistical significance was assessed by ratio paired t test where * indicates $p < 0.05$, ** indicates $p < 0.01$ and *** indicates $p < 0.001$.

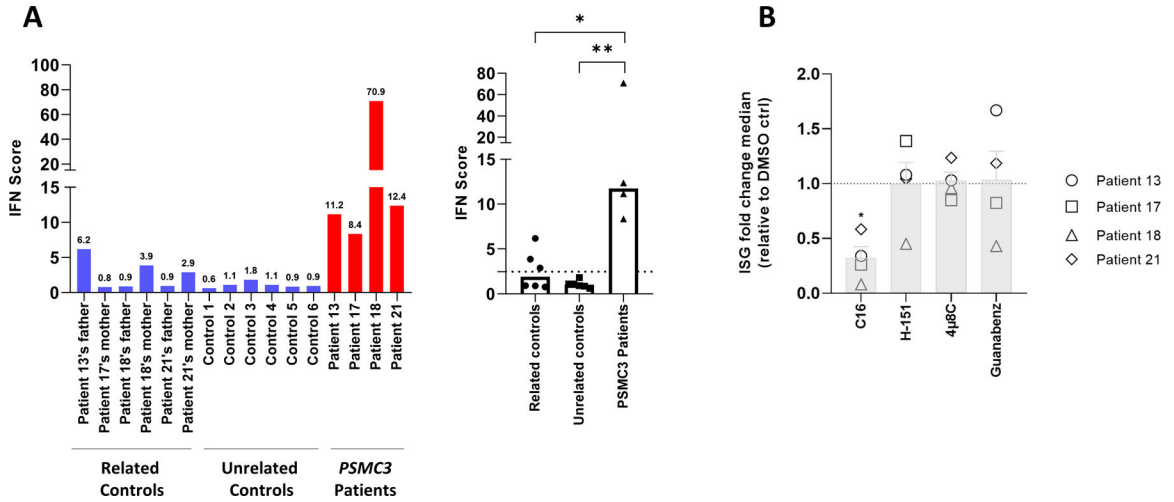


Fig. 8: T cells from patients carrying *PSMC3/Rpt5* variants exhibit high protein kinase R (PKR)-dependent type I IFN scores.

A. Left panel: IFN scores for Patients #13, #17, #18 and #21 and related controls, as well as for six unrelated controls (1 to 6) were calculated as the median of the relative quantifications of the seven ISGs over a single calibrator control. Shown are the IFN scores of each sample (left panel) and the sample groups, namely parents, unrelated healthy donors and patients carrying *PSMC3* variants, as indicated. right panel: Box plot of concatenated data. Statistical significance was assessed by unpaired t test where * indicates $p < 0.05$ and ** indicates $p < 0.001$. **B.** T cells isolated from individuals carrying *PSMC3* variants were subjected to a 6-h treatment with DMSO (vehicle), C16 (500 nM), H-151 (2 μM), 4μ8C (100 μM) or Guanabenz (50 μM) inhibitors before RNA extraction and RT-qPCR for expression analysis of *IFI27*, *IFI44L*, *IFIT1*, *ISG15*, *RSAD2*, *IFI44*, *OASL* and *MX1*. Transcript expression was normalized to *GAPDH* and data are presented as the foldchange median values of the eight ISG relative to DMSO (gridline) for each patient in each treatment. Columns indicate the foldchange mean values ± SEM of the patient group (n=4) for each treatment. Statistical significance was assessed by ratio paired t test where * indicates $p < 0.05$.

Table 1.

Main characteristics of the *PSMC3* *de novo* variants[‡] identified in the patients included in the study.

Chromosomal localization (Chr11/GRCh37)	cDNA change ¶	Protein change	Variant database †	CADD Phred score (v1.6)	Meta-dome	Mobi-Details ‡	Effect on neuronal development	Effect on PSMC3 stability	Effect on proteasome assembly	Effect on mitophagy	IFN signature	Number of patients with the variant
g.474445677G>A	c.511C>T	R171W	rs775517283	27.3	I	45364	improvement	Decrease	ND	ND	ND	1
g.474445665T>C	c.523A>G	M175V	Absent	23.4	I	45365	ND	none	ND	ND	ND	1
g.474444430G>A	c.686C>T	P229L	Absent	25.5	I	195979	ND	ND	ND	ND	ND	1
g.47444406G>A	c.710C>T	A237V	Absent	26.9	HI	45366	ND	Decrease	ND	ND	ND	1
g.47444234T>C	c.775A>G	M259V	Absent	23.4	I	45367	ND	none	ND	ND	ND	1
g.47444233A>G	c.776T>C	M259T	Absent	24.7	I	45368	ND	Decrease	ND	ND	ND	1
g.47444227A>G	c.782T>C	I261T	Absent	24.6	I	45369	ND	Decrease	ND	ND	ND	6
g.47444225C>T	c.784G>A	G262R	Absent	26.8	I	45370	ND	none	none	increase	moderate	1
g.47444203C>G	c.806G>C	R269P	Absent	24	I	45371	ND	Decrease	ND	ND	ND	1
g.47444150C>G	c.859G>C	E287Q	Absent	26.7	I	45372	ND	Decrease	ND	ND	ND	1
g.47442253G>A	c.910C>T	R304W	rs1363348500	31	I	45373	impairment	none	impairment	increase	strong/ very strong	4
g.47442253G>C	c.910C>G	R304G	Absent	28.2	I	45374	ND	none	ND	ND	ND	1
g.47442248C>A	c.915G>T	E305D	Absent	23.1	I	45375	impairment	none	impairment	increase	moderate	1
g.47442234A>G	c.929T>C	M310T	Absent	26.2	HI	45376	ND	none	ND	ND	ND	1
g.47440729C>T	c.1147G>A	E383K	Absent	27.8	N	45377	impairment	none	ND	ND	ND	1

¶ All variants presented are *de novo*, except variant c.775A>G that is suspected *de novo*.

† RefSeq transcript used for *PSMC3* is NM_002804.4; ‡ gnomAD V3, dbSNP v154, ClinVar v20210828; † The access to detailed predictions for variant XXXXX (5364, 45365...) is as follows: <https://mobidetails.iurc.monip.inserm.fr/MD/api/variant/XXXXX/browser/>

ND: not determined; IFN: interferon; I= intolerant; HI= highly intolerant; N= neutral

Table 2.

List of proteins enriched in Patients 17 and 21 versus their controls (mother and father/mother, respectively)

PG-Protein Groups	Protein name	Gene name	Mut/Colsignal_log2_ratio	Mut/Colraw_p_value	Mut/Coladjusted_p_value
P02749	Beta-2-glycoprotein 1	<i>APOH</i>	3,90875773	3.9233E-05	0.01752392
P01861	Immunoglobulin heavy constant gamma 4	<i>IGHG4</i>	3,41081457	3.9313E-07	0.0003951
Q02878	60S ribosomal protein L6	<i>RPL6</i>	3,09519982	8.1083E-05	0.02173071
P62424	60S ribosomal protein L7a	<i>RPL7A</i>	2,97520531	2.4946E-06	0.00143263
P18124	60S ribosomal protein L7	<i>RPL7</i>	2,90834996	5.5264E-05	0.01815176
P83731	60S ribosomal protein L24	<i>RPL24</i>	2,78639617	5.8732E-05	0.01815176
P16403	Histone H1.2	<i>H1-2</i>	2,72232694	4.4042E-05	0.0177049
P02768	Serum albumin	<i>ALB</i>	2,64236248	3.3722E-18	1.3556E-14
P36578	60S ribosomal protein L4	<i>RPL4</i>	2,50022766	3.276E-07	0.0003951
P01876	Immunoglobulin heavy constant alpha 1	<i>IGHA1</i>	2,32067402	3.007E-05	0.01511011
P20591	Interferon-induced GTP-binding protein Mx1	<i>MX1</i>	2,20162951	6.3215E-05	0.01815176
Q6P2Q9	Pre-miRNA-processing-splicing factor 8	<i>PRPF8</i>	1,33941179	1.5549E-06	0.00125012
Q01469	Fatty acid-binding protein 5	<i>FABP5</i>	-2,29088412	5.7962E-05	0.01815176